SOURCE, COMPOSITION, AND BIODEGRADABILITY OF DISSOLVED ORGANIC MATTER IN THE PARLUNG ZANGBO RIVER IN SOUTHERN TIBET, CHINA

by

OLIVIA MARIE WARREN

YUEHAN LU, COMMITTEE CHAIR
CHUNMAIO ZHENG, COMMITTEE CO-CHAIR
FRED ANDRUS
GEOFFREY TICK
XINGXING KUANG

A THESIS

Submitted in partial fulfillment of the requirements
for the degree of Master of Science in Geology
in the Department of Geological Sciences
in the Graduate School of
The University of Alabama

TUSCALOOSA, ALABAMA

2019

ABSTRACT

Regions of the Tibetan Plateau are experiencing increasing temperatures and decreasing glacial mass at a faster rate than the global average. Our study area, the Parlung Zangbo River basin, is within the southeastern region of the Tibetan Plateau which is experiencing the greatest degree of glacial mass loss. Glacial loss could mobilize organic matter from the terrestrial landscape to lakes and rivers and thereby influence watershed carbon cycles, water quality, and aquatic ecological functioning. However, the present-day dissolved organic matter (DOM) pool of the river, which could serve as a baseline for future predictions, has not been characterized. This project will characterize spatial distribution of the amount, source, and biodegradability of DOM exported from the Parlung Zangbo River basin. Samples were collected along the main stem of the river over 170 km, nearby tributaries, and a headwater lake and analyzed for DOC concentration and DOM quality based on absorbance and fluorescence properties. The excitation emission matrix coupled with parallel factor analysis (EEM-PARAFAC) yielded three humic-like fluorophores and two protein-like fluorophores. A subset of samples analyzed with Fourier Transform Ion Cyclotron Resonance Mass Spectrometry (FT-ICR-MS) analysis showed that the DOM pool was dominated by lignins. Incubation experiments showed microbial utilization of DOM increased with increasing temperature up to an optimum temperature (between 17°C and 25°C) before declining. Lake samples showed characteristics indicative of glacial contribution, including greater proportions of Nitrogen-rich DOM and microbially-derived DOM, as well as higher β:α values that suggest lower degrees of diagenesis and higher bioreactivity. Our results suggest that increasing glacial loss in the future may shift the composition and increase the

bioreactivity of DOM pool in Tibetan rivers. Consequently, these shifts in the DOM pool will contribute to global warming through a positive feedback loop.

LIST OF ABBREVIATIONS AND SYMBOLS

YZR	Yarlung Zangbo River
YZRB	Yarlung Zangbo River Basin
PZRB	Parlung Zangbo River Basin
DOM	Dissolved Organic Matter
DOC	Dissolved Organic Carbon
$SUVA_{255}$	Specific Ultraviolet Absorbance at 255 nm
S_R	Spectral Slope Ratio
E2:E3	Absorption Ratio 249 to 399 nm
FI	Fluorescence Index
HIX	Humification Index
β:α	Freshness Index
EEM	Excitation Emission Matrix
PARAFAC	Parallel Factor Analysis
FT-ICR-MS	Fourier Transform Ion Cyclotron Resonance Mass Spectrometry
GR	Guaranteed Reagent
HPLC	High Performance Liquid Chromatography
PCA	Principal Component Analysis

ACKNOWLEDGMENTS

I would like to thank my advisors Drs. Chunmiao Zheng and Yuehan Lu for all they have done to help me through the past two years. I would also like to thank my committee members Drs. Geoffrey Tick and Xingxing Kuang for their insights. Many thanks to Dr. Ding He of Zhejiang University for DOC analysis, Dr. Bin Jiang of Guangzhou Institute of Geochemistry for FT-ICR-MS analysis and interpretation, Yuqin Sun for assistance with Aqualog, and many students of Southern University of Science and Technology for their help with lab equipment. Finally, I would like to thank my lab members at the University of Alabama, Shuo Chen, Peng Shang, Man Lu, Xiaorui He, Mary Hastings Puckett, and Jian Chen for their support.

CONTENTS

LIST OF TABLES

LIST OF FIGURES

INTRODUCTION

The Yarlung Zangbo River (YZR) is the largest river on the Tibetan Plateau in both length and drainage area (Huang et al., 2009a), and supplies water to hundreds of millions of people (Huang et al., 2009b). Over the past three decades, climate shifts including rapid warming, moistening, solar dimming, and wind stilling have been recorded on the Tibetan Plateau (Yang et al., 2014). All these shifts suggest widespread changes in water and energy cycles on the plateau. The need to understand how a changing environment will impact the YZRB has propelled multiple studies in the region. Yao et al. (2010) outlined variation in glacial distribution and glacial mass balance in the YZRB, showing the snow line elevation of glaciers is decreasing gradually, and as a result, glacial-fed lakes and glacial moraine lakes have been expanding. Shi et al. (2011) note greater discharge of the YZRB in recent years resulting from melting glacier and snow coverage. Liu et al. (2012) find that increased human activity and climate change are ultimately increasing runoff to the YZR through increased desertification, decreased grassland, increased reforestation, and retreat of glaciers.

The Parlung Zangbo River, a tributary to the YZR, will be the focus of this study. The fastest shrinking glacier on the Tibetan Plateau has been observed within the Parlung Zangbo River Basin (PZRB) with an average mass balance of -1,698 mm yr^{-1}. The glacier will disappear in the next 25-35 years if the shrinking rate remains constant (Yao et al., 2012). Characterizing the present-day conditions of the Parlung Zangbo River is essential to understanding and predicting the response of the river system to shrinking glaciers, increasing snowmelt, and increasing temperatures.

This project is aimed to evaluate the present-day characteristics of dissolved organic matter (DOM) in the Parlung Zangbo River. DOM is one of the largest organic carbon pools in aquatic ecosystems and plays a pivotal role in regional and global carbon cycles (Hansell and Carlson 2002; Jaffé et al., 2008; Dubnick et al., 2010). DOM is a heterogeneous assortment of compounds including carbohydrates, lipids, proteins, humic and fulvic acids (Singh et al., 2013). DOM is fundamental to ecosystem functioning via serving as a nutrient and energy source to aquatic food webs, attenuator of harmful UV rays, and transporter of heavy metals (Stedmon et al., 2006; Hansen et al., 2016; Raymond et al., 2016). Both quantity and quality of DOM present in aquatic environments impacts key processes including microbial degradation, the biogeochemical cycling of carbon, nitrogen, phosphorous, and sulfur, and energy transfer in aquatic food webs (Jaffé et al., 2008; Lu et al., 2013; Singh et al., 2013). Human land use and climatic factors influence DOM quantity and quality (Wilson and Xenopoulos, 2009; Lu et al., 2013; Creed et al., 2018; Shang et al., 2018). With DOM playing such a central role in energy and substrate cycles, DOM has been considered as a "Master Variable" that mediates water quality and ecological health. Increases in glacial loss and snowmelt propelled by climatic shifts exert notable fluctuations on biogeochemical cycles in nearby streams with far-reaching implications downstream. Over long periods of time, glaciers accumulate organic and inorganic nutrients that become locked in the ice (Fountain et al., 2012; Milner et al., 2017). While DOC concentrations in glacial runoff are low, DOC locked in glacial ice has been shown to be extremely bioavailable, and DOC shunted to a river from a period of glacier melting can promote carbon cycling within the river (Milner et al., 2017). Glacial runoff is a source of dissolved organic nitrogen (DON) and dissolved inorganic nitrogen (DIN), and consequently, glacial loss shunts N-rich DOM to rivers (Hood and Berner, 2009; Milner et al., 2017). During ice breakup

from melting glaciers, the ice can scour the landscape picking up allochthonous detrital material and other nutrients that will subsequently be shunted to rivers (Fountain et al., 2012). With materials and nutrients supplied by glacial melt coming from within the ice and the landscape below the glacier, inputs of DOM from glacial melt are diverse, containing proteinaceous molecules, lignins, and tannins (Milner et al., 2017).

Here, I aim to answer three main research questions: (1) what are the source-composition characteristics of the present-day DOM pool of the Parlung Zangbo River, (2) are there signatures of glacial melt contribution to the surface water DOM pool, and (3) how will increasing temperature alter the composition and bioreactivity of DOM? The goal of this study is to characterize DOM of the Parlung Zangbo River, determining the spatial variability in the amount, source, and biodegradability as well as evaluating the potential of DOM as a tool for predicting the impact of future changes to the river ecosystem. To achieve this, samples were collected from the main stem of the Parlung Zangbo River, nearby tributaries along the river, and a headwater lake. These samples were analyzed for DOC concentration and DOM quality via optical measurements: absorbance and fluorescence. Optical measurements were chosen as the primary tool to investigate the characteristics of DOM in our samples because the method is time and cost efficient and has been shown to offer insight similar to that of molecular level techniques (Fellman et al., 2010; Lu et al., 2015a). A subset of samples from the main stem, tributaries, and headwater lake were collected for molecular level DOM characterization via FT-ICR-MS analysis and for incubation experiments to assess the impact of temperature on DOM availability to microbes.

Background

Study sites

Located on the Tibetan Plateau, the YZR begins at 5,200 m above sea-level from the Jemayangdrung glacier and runs East until it bends southward to reach the Bay of Bengal in the Indian Ocean. The river stretches 2,057 km in length and 240,480 km^2 in area (Yao et al., 2010). The upstream region is characterized by alpine meadow with annual precipitation of < 300 mm; the midstream region is characterized by alpine grassland with annual precipitation of 300 – 600 mm, and finally, the downstream region is characterized by alpine forest with annual precipitation of > 2000 mm (Liu et al., 2012). The river transitions from running through narrow gorges near its headwaters at the Jemayangdrung glacier, to wide open fluvial valleys in fertile plains along its mid-reaches, to deep gorges in a densely forested area along its lower reaches, until it finally flows into the Bay of Bengal (Huang et al., 2009a). Bedrock along the YZR is made up primarily of granite gneiss, schist, and volcanic rock with some sedimentary and metamorphosed sedimentary units; ophiolites are common along the river because it trends along the Indus-Yarlung suture zone (Huang et al., 2009a). The YZRB has an average elevation of 4,600 m above sea-level, making it one of the highest river basins in the world and an important location for precipitation generation as moisture from the Indian Ocean reaches the basin (Liu et al., 2012). The river basin experiences distinct wet and dry seasons: May to September and October to April, respectively (Li et al., 2014). The YZRB contains 10,816 glaciers, the highest number of glaciers found in the exorheic basins of China, with 1,293 km^3 in ice volume (Yao et al., 2010). Glacier snow melt has been estimated to cause increase in runoff ranging from 1.7 mm/10 yr to 6.0 mm/10 yr (Liu et al., 2012). The YZR has an average annual runoff of 165 billion m^3 (Huang et al., 2009a).

The Parlung Zangbo River is a major tributary to the YZR. Namely, it is the largest contributor based on water discharge to the YZR (Huang et al., 2009b). The Parlung Zangbo River originates from the Laigu glacier and flows west until reaching the Yilong Zangbu River where the river turns south to merge with the YZR (Zhou et al., 2007). The river runs 266 km over the Tibetan Plateau with a total catchment area of 28,631 km^2 (Huang et al., 2009b). The average annual flow rate of the river has been measured as 421 m^3/s (Choi et al., 2018). The Parlung Zangbo River is primarily supplied by maritime glaciers and snowmelt (Huang et al., 2009b). Yao et al. (2010) observe 1,378 glaciers in the PZRB with a total volume of 268.33 km^3 and an area of 2703.74 km^2.

Dissolved organic matter

DOM in aquatic environments can be classified based on origin as either autochthonous, produced in situ through phytoplankton production or through decomposition of bacterial and algal matter, or allochthonous, transported terrestrial plant and soil matter (McKnight et al., 2003; Lu et al., 2013; Sankar et al., 2018). Autochthonous DOM is observed to be enriched in aliphatic carbon and organic nitrogen compared to allochthonous DOM, and allochthonous DOM is observed to be enriched in aromatic carbon (Brandão et al., 2018). The differences in composition between autochthonous and allochthonous DOM are important for degradation rates and bioavailability. Allochthonous DOM, typically made of larger more aromatic compounds, absorbs more ultraviolet light and is more susceptible to photodegradation, and autochthonous DOM, typically made of lower molecular weight molecules, is more labile to the microbial community (Brandão et al., 2018).

Both quantity and composition of DOM in streams is dynamic. Some drivers of fluctuations include land use, watershed characteristics, hydrological events, seasonal variability,

and environmental processing. Lu et al. (2013) find amounts and characteristics of DOM are distinctly different between forested and human-modified watersheds. Watersheds with higher slopes tend to have lower DOC concentrations (Shang et al., 2018). During high-discharge events from either rainfall or snowmelt, high volumes of terrestrial DOM enters streams, quickly traveling downstream and altering the diversity and quantity of DOM (Raymond et al., 2016). Similarly, during seasonal changes, high inputs of leaf litter can alter the balance of autochthonous to allochthonous DOM. DOM degradation rates also alter the DOM profile of streams and can be influenced by the following factors: available sunlight, chemical characteristics of DOM, bioavailability, microbial community present, and presence of inorganic nutrients, namely phosphorous and nitrogen (Brandão et al., 2018).

Techniques to characterize DOM are fundamental to understanding its role in aquatic ecosystems. A rapid, low cost approach to characterizing DOM composition involves the use of the optical measurements, fluorescence and ultraviolent-visible absorption spectroscopy (Singh et al., 2013; Hansen et al., 2016; Shang et al., 2018). From these measurements, several optical indices are used to describe DOM quality including specific ultraviolet absorbance (SUVA), spectral slope ratio (S_R), freshness index (β:α), fluorescence index (FI), and humification index (HIX) (Singh et al., 2013; Hansen et al., 2016). In addition to indices, the fluorescence measurements are compiled into an excitation-emission matrix (EEM), which displays fluorophore intensity with a series of measurements of light emitted over range of wavelengths from excitation at a series of known wavelengths (Dubnick et al., 2010). EEMs can be used to describe DOM origin, chemistry, reactivity, and ecological function (Stubbins et al., 2014). Parallel factor analysis (PARAFAC) can be applied to EEMs to distinguish fluorophores into individual components (Dubnick et al., 2010; Lu et al., 2013). The individual components can be

associated to DOM fractions based on peak fluorescence intensity. Previous studies show DOM interpretations from optical measurements are comparable to interpretations from molecular level measurements (Fellman et al., 2010; Lu et al., 2015a). An approach to molecular level characterization of DOM involves the use of Fourier transform ion cyclotron resonance mass spectrometry (FT-ICR-MS). Through solid-phase extraction, DOM is isolated to highly concentrated organic samples that can be used for FT-ICR-MS analysis. Identification of ionized organic compounds with FT-ICR-MS can provide detail and diversity of DOM compounds that may be missed with optical measurements alone (Lu et al., 2015b). Thousands of peaks from a single DOM samples can be identified with FT-ICR-MS and subsequently be assigned elemental formulas (Stubbins et al., 2014).

METHODOLODY

Sample Collection

Samples were collected in July 2018 in duplicate from a total of 90 sampling sites along the Parlung Zangbo River from approximately 170 km along its main stem, nearby tributaries, and headwater lake (Figure 1). A suite of in situ parameters was measured during sampling (Table 1). Stream water samples were collected in 2 L acid-washed polycarbonate bottles and stored on ice in the dark until filtration at a temporary field laboratory. Samples were filtered through pre-combusted Whatman GF/F glass fiber filters (pore size 0.7 um, pre-combusted at 500ºC for 5h) and stored in the dark at -20 ºC in 30 mL HDPE bottles for DOM quality and DOC analysis. Two 2 L of raw water from 22 sampling locations were brought back to the Southern University of Science and Technology and preserved at -20 ºC for FT-ICR-MS analysis and incubation experiments.

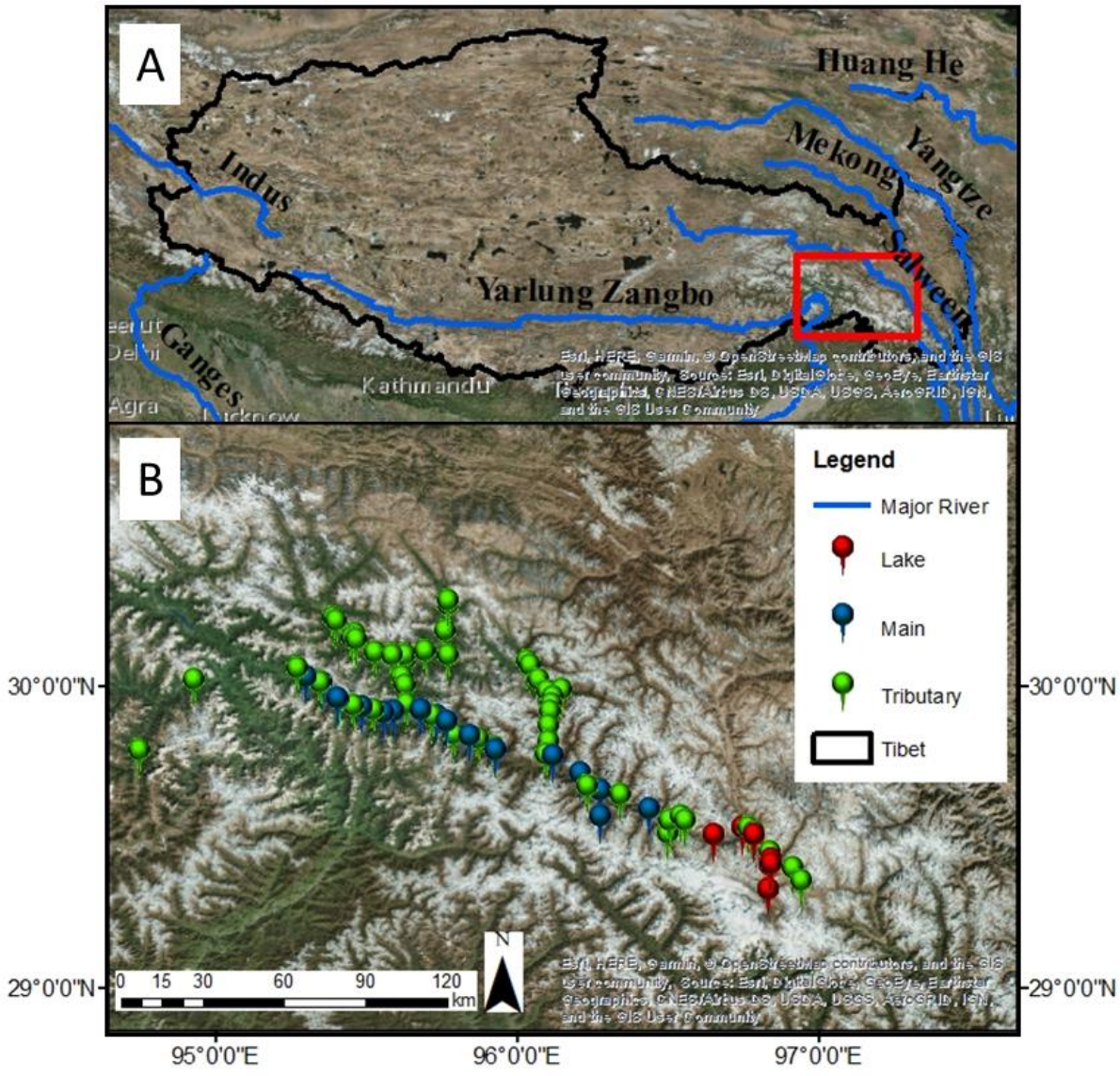

Figure 1: A) Study site delineated in red. B) Sampling sites indicted by poles. Map created in ArcGIS.

Table 1: Average ± standard deviation in situ measurements. Number of sample sites listed in parentheses. Note: some sampling sites missing data for each parameter.

	Elevation (m)	Water Temperature (°C)	Air Temperature (°C)	pH	DO (mg/L)	Electrical Conductivity (µS/cm)	Oxidation Reduction Potential (mV)
All Samples	3058.3 ± 499.5 (60)	11.1 ± 3.4 (81)	16.9 ± 3.8 (71)	8.3 ± 0.4 (82)	7.7 ± 1.8 (81)	174.7 ± 205.5 (63)	91.9 ± 26.4 (82)
Main	2797.1 ± 306.0 (16)	12.6 ± 3.1 (20)	16.5 ± 2.9 (19)	8.1 ± 0.5 (21)	7.8 ± 2.6 (21)	289.1 ± 344.2 (21)	71.2 ± 22.2 (21)
Tributary	3020.0 ± 449.4 (37)	10.4 ± 3.4 (54)	17.3 ± 4.3 (46)	8.4 ± 0.2 (54)	7.9 ± 1.2 (53)	126.4 ± 94.9 (54)	97.9 ± 25.2 (54)
Lake	3892.4 ± 34.4 (7)	12.7 ± 3.3 (7)	15.4 ± 2.0 (6)	8.4 ± 0.5 (7)	5.4 ± 1.6 (7)	204.3 ± 165.8 (7)	107.7 ± 7.6 (7)

DOC Concentration

DOC concentration was measured at Zhejiang University using a Shimadzu TOC-V total organic carbon analyzer. The calibration curve was constructed using potassium hydrogen phthalate solutions with six known concentrations. Carbon free ultrapure water was measured regularly to assess instrumental baseline. The relative standard of deviation was within 3 – 5 % based on 2 – 3 measurements of each sample. During DOC measurements, 36 lab used standards (0.15 mg/L) were analyzed with an average value of 0.14 ± 0.02 mg/L.

DOM Quality

Absorbance and fluorescence measurements were made on a Horiba Scientific Aqualog Fluorometer at the Southern University of Science and Technology using the following parameters: scanning wavelength 240-600 nm, increment 2.33 nm, and integration time 1 sec. Due to instrument setting of increment at 2.33 nm, indices were calculated with the closest nm measurement to traditionally defined values, e.g., $SUVA_{255}$ in place of $SUVA_{254}$. Samples were analyzed at room temperature using a 10-mm path length quartz cuvette cleaned with ultrapure carbon-free water six times in-between samples. The optical properties of DOM provide information on both its source and compositional characteristics, providing a substitute for higher cost, time-intensive molecular level techniques (Fellman et al., 2010; Lu et al., 2015a; Hansen et al., 2016).

Specific ultraviolet absorbance at 255 nm ($SUVA_{255}$ (L mg-$C^{-1}m^{-1}$) was calculated as the absorption coefficient at 255 nm divided by DOC concentration (Hansen et al., 2016). Spectral slope ratio (S_R) was calculated as the spectral slope of 276-294 (nm^{-1}) divided by spectral slope

of 351-399 (nm^{-1}) (Hansen et al., 2016) Spectral slope was defined following Shang et al. (2018) relative to the reference wavelength (λ_{ref}) using the following equations:

$$a_\lambda = \frac{2.303 \times A_\lambda}{1}$$

$$a_\lambda = a_{\lambda ref} \times e^{-Sx(\lambda - \lambda ref)}$$

where a_λ=absorption coefficient (m^{-1}) at the wavelength of λ, A_λ=absorption coefficient at wavelength λ and 1= path length (m) (Shang et al., 2018; Spencer et al., 2007). E2:E3 (249/399) was calculated as the ratio of absorbance at 249 to 399 nm (De Haan and De Boer, 1987).

DOM fluorescence property determined using the drEEM toolbox (0.3.0) with the excitation-emission matrix (EEM) to perform parallel factor analysis (PARAFAC) in MATLAB (Murphy et al., 2013). Inner-filter effect and Raman curve corrected with Aqualog software. The PARAFAC modelwas validated using split-half analysis by randomly assigning samples into four quarter splits and performing three validation tests on the six combined dataset halves (Murphy et al., 2013; Shang et al., 2018). 179 samples were included in the model, and 4 outliers were removed from the model.

Freshness Index (β:α) was calculated as the ratio of emission intensity at 380.76 nm divided by the maximum emission intensity between 419.82 nm and 435.97 nm at excitation 309 nm (Hansen et al. 2016). Fluorescence Index (FI) was calculated as the ratio of emission wavelengths at 470.68 nm and 519.54 nm found at excitation wavelength 369 nm (McKnight et al., 2001; Cory et al., 2010; Hansen et al., 2016). Humification Index (HIX) was calculated as the area under the emission spectra from 435.97-479.96 nm divided by the peak area 301.13-344.24 nm plus 435.97-479.96 nm at excitation wavelength 255 nm (Hansen et al., 2016).

FT-ICR-MS Analysis

3.5 L of raw water samples was filtered through pre-combusted Whatman GF/F glass fiber filters (pore size 0.7 um, pre-combusted at 500ºC for 5h) using a geopump (Geotech Environmental Equipment, Inc.). Sample filtrates then used for SPE-DOM extraction following protocol outlined by Dittmar et al. (2008). Before extraction, all samples were acidified to a pH 2-3 (approximately 0.5 mL guaranteed reagent (GR) grade HCL to 2 L sample). Agilent 50 mg cartridges were used for extraction. Cartridges were conditioned by first filling with methanol, allowing it to drain by gravity, and then repeated twice with acidified ultrapure carbon-free water. Acidified samples passed through cartridges with a flow rate of approximately 40 mL/minute maintaining pressure at 10-11 m Hg. Once all 3.5 L of sample passed through the cartridge, the cartridge was rinsed three times with one cartridge volume of 0.01 M HCL to remove salt. Cartridges were allowed to dry before being wrapped in pre-combusted aluminum foil and stored at -20 ºC. One day before Fourier transform ion cyclotron resonance mass spectrometry (FT-ICR-MS) analysis, high performance liquid chromatography (HPLC) grade methanol was used to extract DOM from cartridges. One cartridge volume of methanol was passed through each cartridge and collected in Teflon-lined glass vials stored at -20ºC until FT-ICR-MS analysis.

FT-ICR-MS analysis was performed at the Chinese Academy of Sciences Institute of Geochemistry in Guangzhou, Guangdong, China. The samples were analyzed using a solariX XR FT-ICR MS (Bruker Daltonik GmbH, Bremen, Germany) equipped with a 9.4 T refrigerated actively shielded superconducting magnet (Bruker Biospin, Wissembourg, France) and the Paracell analyzer cell. The samples were ionized in negative ion mode using the ESI ion source (Bruker Daltonik GmbH, Bremen, Germany). The detection mass range was set to m/z 150 –

1000. Ion accumulation time was set to 0.1 s. A total of 128 continuous 4 M data FT-ICR transients were co-added to enhance the signal-to-noise ratio and dynamic range. Field blank filters were processed and analyzed following the same procedure to detect possible contamination. The mass spectra were calibrated externally with arginine clusters in negative ion mode using a linear calibration. The final spectrum was internally recalibrated with typical O_2 class species peaks using quadratic calibration in DataAnalysis 5.0 (Bruker Daltonics). A typical mass-resolving power (m/Δm50 %, in which Δm50% is the magnitude of the mass spectral peak full width at half-maximum peak height) >450 000 at m/z 319 with <0.3 ppm absolute mass error was achieved. The custom software was used to calculate all mathematically possible formulas for all ions with a signal-to-noise ratio > 10 using a mass tolerance of ±1 ppm. The maximum number of atoms for the formula calculator was set to: 30 ^{12}C, 60 ^{1}H, 20 ^{16}O, 3 ^{14}N, 1 ^{32}S, 1 ^{13}C, 1 ^{18}O and 1 ^{34}S. For chemical formula $C_cH_hO_oN_nS_s$, the DBE is calculated using the equation:

$$DBE = (2c + 2\text{-}h + n) / 2.$$

Modified aromaticity index (AI_{mod}) values were calculated with the following formula:

$$AI_{mod} = (1 + c - 0.5o - s - 0.5h) / (c - 0.5o - s - n).$$

Incubation Experiments

Experiment procedure

500 mL of raw water from 18 samples was filtered through pre-baked Whatman GF/F glass fiber filters (pore size 0.7 um, pre-combusted at 500ºC for 5h) using a geopump (Geotech Environmental Equipment, Inc.). Filtrate was stored in 500 mL acid-washed polycarbonate bottles at -20°C in the dark until incubation. At the start of incubation, 7 mL of bacterial inoculum (see below) was added to 70 mL of filtrate from each sample in 150 mL pre-combusted conical flasks and shaken thoroughly; this step is repeated for each sample to create a duplicate for each sample. Blanks, in duplicate, were created with 7 mL of bacterial inoculum added to 70 mL of ultrapure, carbon-free water and shaken thoroughly. At T0, subsamples were taken from each of the 38 flasks (18 samples with duplicates, 2 blanks) for DOM and DOC measurements. Subsamples were filtered through pre-baked GF/F glass fiber filters before preservation for analysis. DOM and DOC samples were stored at -20°C in the dark until analysis. After taking T0 subsamples, the remaining 40 mL of each sample in the flasks was covered with pre-combusted aluminum foil, using needle to make fine holes on the aluminum foil lids for oxygen penetration. The covered flasks were then placed in the incubator set at 11°C for five days. On day 5, subsamples were taken from each flask for DOM and DOC analysis. Subsamples were filtered through pre-baked GF/F glass fiber filters before preservation for analysis using the same method as described for T0 subsamples. The entire incubation procedure was repeated, as described above, at temperature 25°C and carried out simultaneously with the experiment at 11°C using the same bacterial inoculum for both sets of experiments. Next, the entire incubation procedure was repeated at temperature 17°C after these first two experiments were completed due to space limitations using a freshly prepared bacterial inoculum created from the same soil.

Bacterial inoculum preparation

To prepare the bacterial inoculum, 150 g of sieved, moist soil was combined with 750 ml of ultrapure, carbon-free water, gently shaken for 10 minutes, and then allowed to settle overnight. Next, the bacterial inoculum was filtered through pre-combusted Whatman GF/F filter, transferred to an acid-washed polycarbonate bottle, diluted 1:1 with ultrapure, carbon-free water, and incubated at room temperature for 24-48 hours before addition to the sample in 1:10 proportions by volume.

Statistical Analysis

All statistical analysis was performed with XLSTAT (2019.1.2). Non-parametric, Spearman correlation tests were performed to evaluate correlation the between two variables with $p<0.05$. Kruskal-Wallis tests were performed to evaluate the significant differences with $p<0.05$. Following Kruskal-Wallis tests, Dunn's tests were performed to determine which pairs were significantly different. Principle Component Analysis (PCA) was performed using Pearson's correlation matrix. Variables included in the PCA were selected based on the Kaiser-Meyer-Olkin test (>0.5) to test for sampling adequacy and Bartlett's test of sphericity ($p<0.5$) to test for intercorrelation between variables without extreme multicollinearity. Variables were standardized for PCA, and PCA factors with eigenvalues > 1.5 were selected.

RESULTS

DOM Characterization

DOC concentrations in our samples are highly variable ranging from 0.29 to 23.92 mg/L. DOC average concentration is highest in Tributary samples (3.92 ± 5.23 mg/L), followed by Main samples (2.28 ± 5.36 mg/L) (Figure 2; Table 2). While the DOC average concentration of Lake samples (1.04 ± 2.34 mg/L) is the lowest of the three, it is not statistically different from either grouping. DOC concentrations in rivers typically fall within the range of 0.5 to 50 mg/L (Stubbins et al., 2014). The DOC average concentrations for our samples fall on the lower end of this typical range.

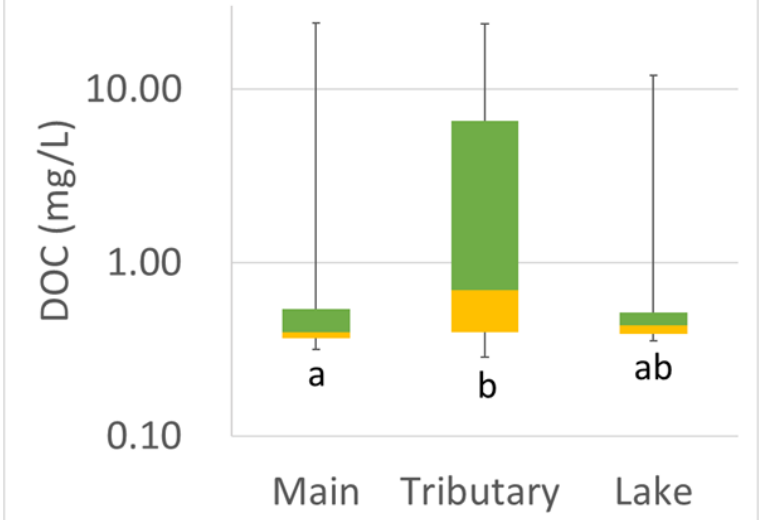

Figure 2: DOC concentrations (mg/L) on a logarithmic scale. Values are significant based on Kruskal-Wallis test ($P<0.05$). Significantly different pairs based on Dunn's test are indicated by different letters..

Table 2: Average ± standard deviation of DOC and absorbance and fluorescence indices. Sample size, including duplicates, listed in parentheses.

	DOC (mg/L)	SUVA255 (L mg-C^{-1}m^{-1})	SR	E2:E3	β:α	FI	HIX
All Samples	3.08 ± 5.05 (182)	10.71 ± 19.92 (174)	1.45 ± 0.75 (174)	3.31 ± 3.28 (174)	0.95 ± 0.40 (182)	1.72 ± 0.45 (182)	0.49 ± 0.14 (182)
Main	2.28 ± 5.36 (47)	7.86 ± 8.49 (46)	1.17 ± 0.22 (46)	3.36 ± 2.10 (46)	1.01 ± 0.31 (47)	1.64 ± 0.16 (47)	0.50 ± 0.14 (47)
Tributary	3.92 ± 5.23 (108)	5.95 ± 13.48 (101)	1.61 ± 0.91 (101)	3.40 ± 3.85 (101)	0.83 ± 0.36 (108)	1.77 ± 0.55 (108)	0.49 ± 0.14 (108)
Lake	1.04 ± 2.34 (27)	33.94 ± 33.82 (27)	1.30 ± 0.41 (27)	2.90 ± 2.33 (27)	1.37 ± 0.41 (27)	1.64 ± 0.29 (27)	0.49 ± 0.12 (27)

Absorbance indices provide information on molecular weight, size, and aromaticity. $SUVA_{255}$ and Slope Ratio (S_R) are indicators of molecular weight and aromaticity; specifically, a high $SUVA_{255}$ and a low S_R are indicative of high molecular weight and aromaticity (Hansen et al., 2016; Shang et al., 2018). Lake samples have the highest average $SUVA_{255}$ of 33.94 (± 33.82), followed by statistically similar Main samples with an average of 7.86 (±8.49). Tributary samples have the lowest average $SUVA_{255}$ of 5.95 (±13.48) (Figure 3; Table 2). Large standard deviations for $SUVA_{255}$ values can be attributed to high variability of DOC concentrations. Main samples have the lowest average S_R of 1.17 (±0.22), and Tributary samples have the highest average S_R of 1.61 (±0.91); the average S_R of Lake samples is not statistically different from Main samples. E2:E3 decreases with increasing molecular size (De Haan and De Boer, 1987), and E2:E3 values are lowest in Lake samples with an average of 2.90 (±2.33). E2:E3 is negatively correlated with $SUVA_{255}$ and S_R (Table 3).

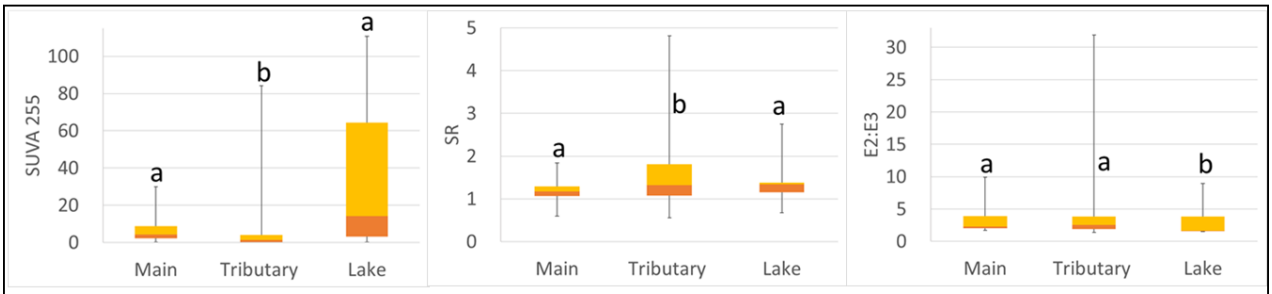

Figure 3: Specific UV absorbance, $SUVA_{255}$ (L mg-C^{-1} m^{-1}); spectral slope ratio of 276–294 nm over 351–399 nm, S_R; and the ratio of absorbance at 249 & 399, E2:E3. Values are significant based on Kruskal-Wallis test ($P<0.05$). Significantly different pairs based on Dunn's test are indicated by different letters.

Table 3: Spearman correlation coefficients for DOM indices and DOC, $p<0.05$. Values in bold indicate the correlation is significant with a significance level of $\alpha=0.05$. Sample size was 171.

	$SUVA_{255}$	S_R	E2:E3	β:α	FI	HIX	$\%F_{C1}$	$\%F_{C2}$	$\%F_{C3}$	$\%F_{C4}$	$\%F_{C5}$	DOC
$SUVA_{255}$		-0.13	**-0.58**	**0.66**	-0.15	**-0.40**	**-0.66**	**0.70**	**-0.53**	**0.36**	**0.66**	**-0.71**
S_R	-0.13		**-0.36**	0.03	**0.33**	-0.02	**-0.21**	0.13	**-0.18**	**0.19**	0.10	**0.29**
E2:E3	**-0.58**	**-0.36**		**-0.51**	-0.03	**0.30**	**0.64**	**-0.81**	**0.64**	**-0.61**	**-0.78**	**0.36**
β:α	**0.66**	0.03	**-0.51**		-0.13	**-0.41**	**-0.79**	**0.73**	**-0.53**	**0.56**	**0.71**	**-0.37**
FI	-0.15	**0.33**	-0.03	-0.13		**0.28**	**0.18**	-0.07	-0.06	**-0.16**	-0.13	**0.35**
HIX	**-0.40**	-0.02	**0.30**	**-0.41**	**0.28**		**0.69**	**-0.25**	-0.14	-0.14	**-0.28**	**0.53**
$\%F_{C1}$	**-0.66**	**-0.21**	**0.64**	**-0.79**	**0.18**	**0.69**		**-0.73**	**0.46**	**-0.65**	**-0.76**	**0.43**
$\%F_{C2}$	**0.70**	0.13	**-0.81**	**0.73**	-0.07	**-0.25**	**-0.73**		**-0.84**	**0.75**	**0.95**	**-0.40**
$\%F_{C3}$	**-0.53**	**-0.18**	**0.64**	**-0.53**	-0.06	-0.14	**0.46**	**-0.84**		**-0.73**	**-0.81**	0.13
$\%F_{C4}$	**0.36**	**0.19**	**-0.61**	**0.56**	**-0.16**	-0.14	**-0.65**	**0.75**	**-0.73**		**0.84**	-0.10
$\%F_{C5}$	**0.66**	0.10	**-0.78**	**0.71**	-0.13	**-0.28**	**-0.76**	**0.95**	**-0.81**	**0.84**		**-0.37**
DOC	**-0.71**	**0.29**	**0.36**	**-0.37**	**0.35**	**0.53**	**0.43**	**-0.40**	0.13	-0.10	**-0.37**	

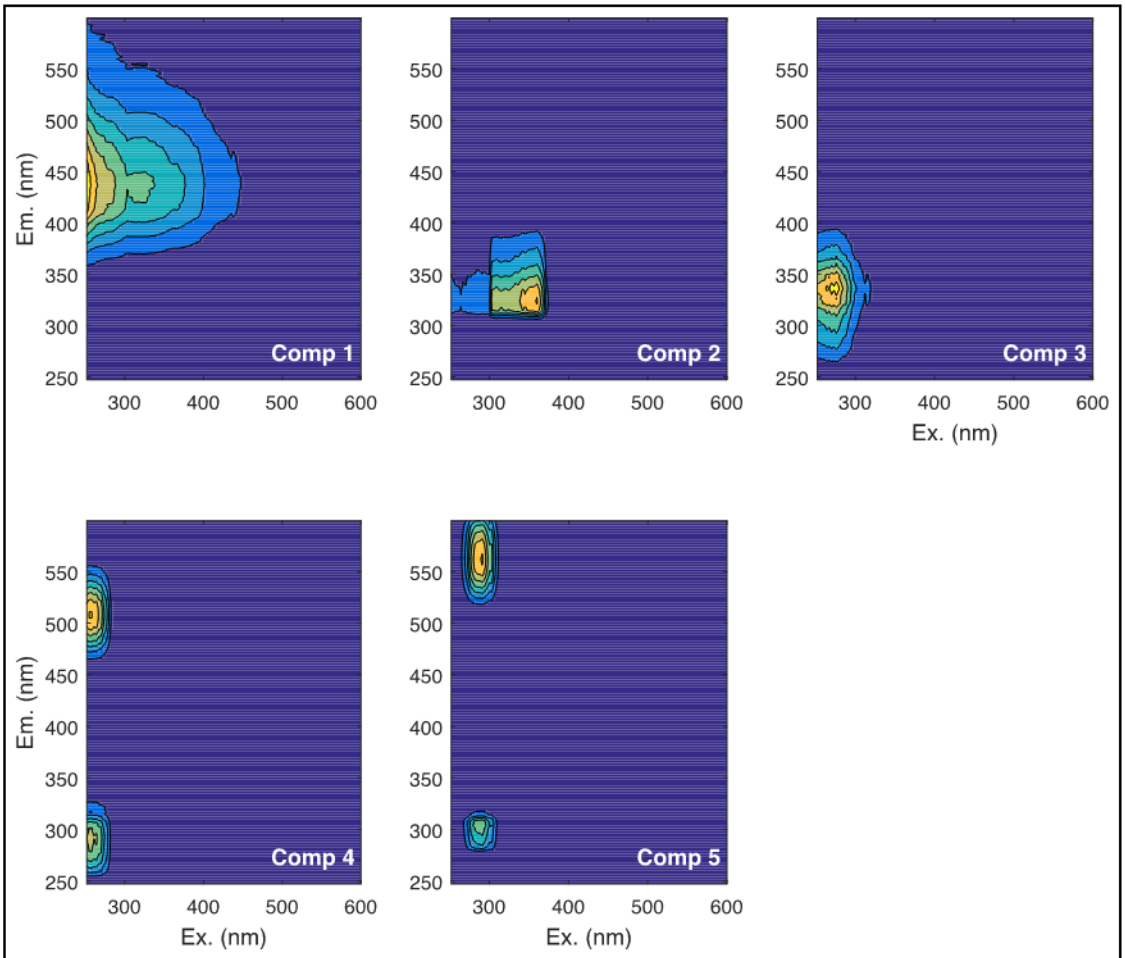

Figure 4: Contour plots of five components based on excitation-emission matrix of Parlung Zangbo main stem river, tributary, and lake water samples.

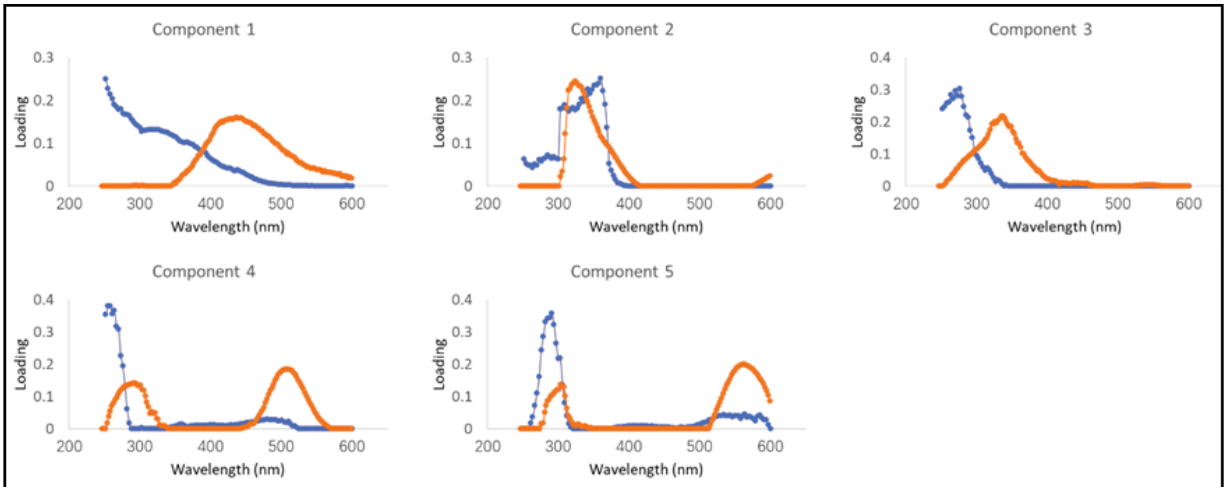

Figure 5: Loading of five fluorescence components from Fig 4.

Table 4: Five identified fluorescence components and their assigned sources.

Component	Excitation Maximum (nm)	Emission Maximum (nm)	Source Assignment in Present Study	Similar Fluorescence Components in Previous Studies
C1	252	436	humic-like	**Coble (2007)**: A (humic-like), **Lu et al. (2015)**: C1 (humic-like, degradation product of OM), **Fellman et al. (2010)**: humic-like
C2	360	324	protein-like, microbial-like	**Dubnick et al. (2010):** soluble microbial byproduct-like
C3	276	335	protein-like, tryptophan-like	**Coble (2007)**: T (tryptophan-like), **Lu et al. (2015)**: C4 (typtophan-like, mostly controlled by diagenesis), **Fellman et al. (2010)**: tryptophan-like
C4	258	508 (292)	humic-like	**Fellman et al. (2010)**: humic-like, **Wünsch et al. (2017)**: humic-like
C5	291	562 (303)	humic-like	**Dubnick et al. (2010)**: humic-like

Five fluorescence components were identified based on the excitation-emission matrix of 178 Parlung Zangbo Main, Tributary and Lake water samples (Figure 4 & 5). Sources were assigned to fluorescence components based on similar components found in previous studies (Table 4). C1 comprises 15.76 ± 0.19% of total fluorescence and is assigned as humic-like compounds (Figure 6; Table 5). C2 comprises 27.35 ± 0.57% of total fluorescence and is assigned as microbially derived protein-like compounds. C3 comprises 28.37 ± 1.56% of total fluorescence and is assigned as tryptophan-like protein compounds. C4 and C5 are both assigned as humic-like compounds comprising 16.08 ± 0.32% and 12.44 ± 0.25%, respectively, of total fluorescence. Excluding C5, Lake samples have statistically different contributions from components compared to Main and Tributary samples (Figure 7). Lake samples have greater contributions of C2 and C4 and lower contributions of C1 and C3 compared to Main and Tributary samples. For C5, contributions of components to total fluorescence are statistically different between Tributary and Lake samples, with Lake samples having greater contributions of C5.

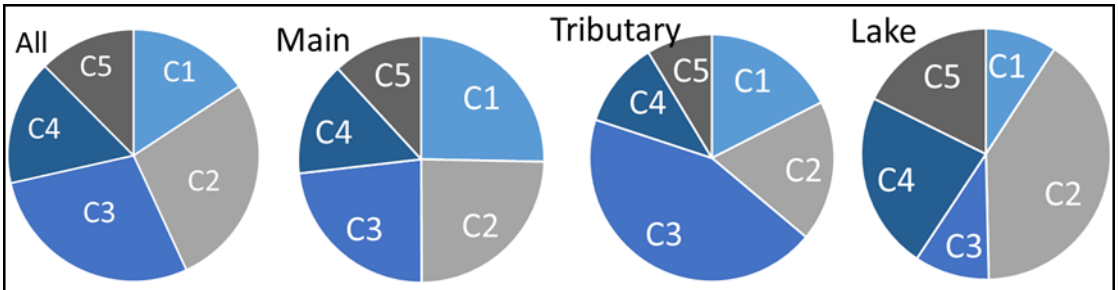

Figure 6: Comparison of percent contribution of identified fluorescence components to total fluorescence of All, Main stem, Tributary, and Lake samples.

Table 5: Contribution percentages (%) ± standard deviations from Fig. 6. Sample size, including duplicates, listed in parentheses.

	All Samples	Main	Tributary	Lake
C1	15.76 ± 0.19 (178)	25.32 ± 0.22 (46)	17.57 ± 0.18 (105)	9.25 ± 0.15 (27)
C2	27.35 ± 0.57 (178)	24.63 ± 0.15 (46)	18.48 ± 0.31 (105)	40.38 ± 1.09 (27)
C3	28.37 ± 1.56 (178)	23.21 ± 0.18 (46)	43.97 ± 1.98 (105)	9.71 ± 0.89 (27)
C4	16.08 ± 0.32 (178)	14.98 ± 0.09 (46)	11.31 ± 0.17 (105)	22.93 ± 0.61 (27)
C5	12.44 ± 0.25 (178)	11.86 ± 0.08 (46)	8.67 ± 0.14 (105)	17.72 ± 0.47 (27)

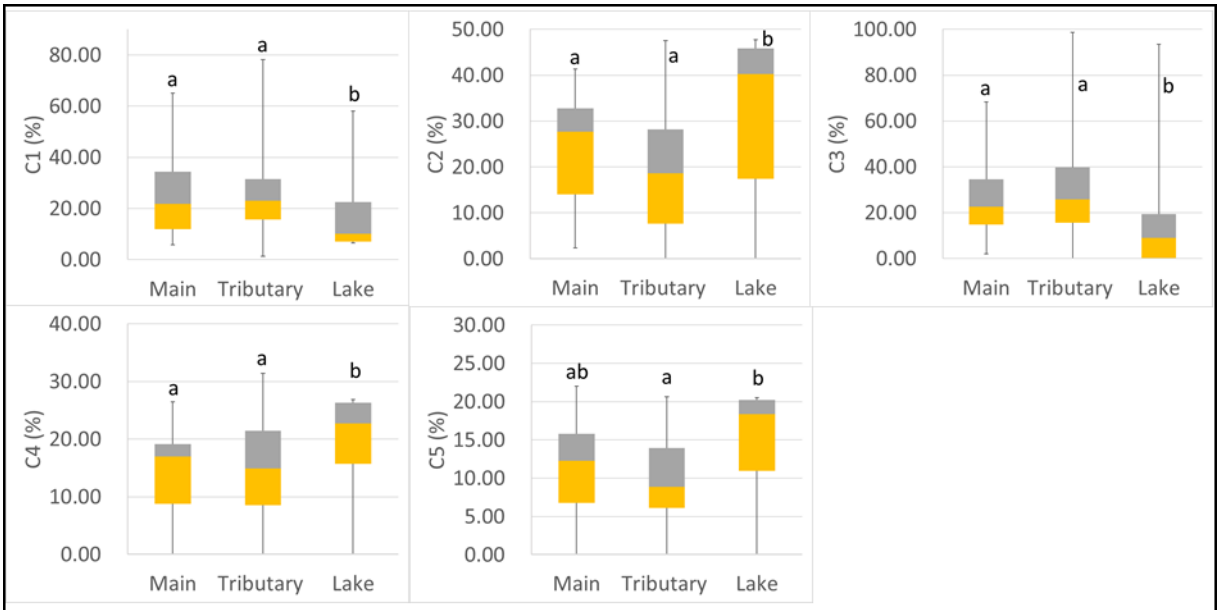

Figure 7: Percent contributions of components to total fluorescence. Values are significant based on Kruskal-Wallis test ($P<0.05$). Significantly different pairs based on Dunn's test are indicated by different letters.

Fluorescence indices provide information on biological origins of DOM. The freshness index (β:α) is an indicator of recently produced DOM, with higher values (> 1) indicating a higher proportion of fresh DOM (Parlanti et al., 2000; Wilson and Xenopoulos, 2009). β:α values were statistically different among all three sample groupings. Lake samples have the highest average β:α value of 1.37 (± 0.41), and Tributary samples have the lowest average of 0.83 (± 0.36), while the Main sample average of 1.01 (± 0.31) falls between the two (Figure 8). FI values typically range near 1.2 for terrestrially dominated DOM and 1.8 for microbially dominated DOM (Jaffe et al., 2008). Although FI values of sample groupings are not statistically different from another, the average FI value for all samples 1.72 (± 0.45) suggests a high proportion of microbial DOM present (Table 2). Huguet et al. (2009) find an HIX < 4 indicates dominance of autochthonous DOM and HIX >16 suggests dominance of terrestrial DOM. The average HIX for all samples of 0.49 (± 0.14) is less than 4, suggesting the dominance of autochthonous DOM (Table 2). HIX values are not statistically different among sample groupings (Figure 8). HIX is positively correlated with FI and negatively correlated with β:α (Table 3).

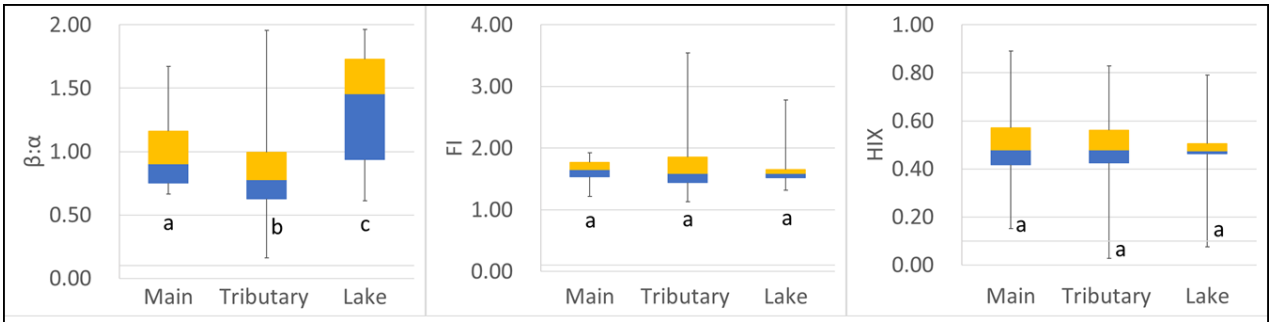

Figure 8: Freshness Index (β:α), Fluorescence Index (FI), and Humification Index (HIX). Freshness values are significant based on Kruskal-Wallis test ($P<0.05$). Significantly different pairs based on Dunn's test are indicated by different letters.

Table 6: Spearman correlation coefficients for DOM indices, DOC, and FT-ICR-MS parameters, $p<0.05$. Values in bold indicate the correlation is significant with a significance level of $\alpha=0.05$. Sample size was 42.

	$SUVA_{255}$	S_R	E2:E3	β:α	FI	HIX	$\%F_{C1}$	$\%F_{C2}$	$\%F_{C3}$	$\%F_{C4}$	$\%F_{C5}$	DOC	% CHO	% CHOS	% CHON	% CHONS	% Lipid	% Protein	% Carb	%UHC	% Lignin	% CAS	DBE	AI_{mod}
$SUVA_{255}$		-0.13	**-0.58**	**0.66**	-0.15	**-0.40**	**-0.66**	**0.70**	**-0.53**	**0.36**	**0.66**	**-0.71**	**-0.41**	**0.33**	0.26	0.05	0.11	**0.41**	0.22	-0.25	**-0.35**	0.17	-0.29	-0.05
S_R	-0.13		**-0.36**	0.03	**0.33**	-0.02	**-0.21**	0.13	**-0.18**	**0.19**	0.10	**0.29**	0.11	-0.23	0.22	-0.13	0.05	0.13	0.10	-0.07	-0.20	0.12	-0.15	0.17
E2:E3	**-0.58**	**-0.36**		**-0.51**	-0.03	**0.30**	**0.64**	**-0.81**	**0.64**	**-0.61**	**-0.78**	**0.36**	0.22	-0.07	**-0.36**	0.08	-0.06	**-0.38**	-0.23	0.03	**0.32**	-0.06	0.20	-0.08
β:α	**0.66**	0.03	**-0.51**		-0.13	**-0.41**	**-0.79**	**0.73**	**-0.53**	**0.56**	**0.71**	**-0.37**	**-0.34**	0.26	0.20	0.02	0.17	**0.35**	0.17	-0.13	-0.26	-0.01	-0.28	-0.14
FI	-0.15	**0.33**	-0.03	-0.13		**0.28**	**0.18**	-0.07	-0.06	**-0.16**	-0.13	**0.35**	-0.11	0.16	0.15	0.00	0.16	**0.42**	**0.40**	-0.02	**-0.46**	-0.12	-0.25	-0.08
HIX	**-0.40**	-0.02	**0.30**	**-0.41**	**0.28**		**0.69**	**-0.25**	-0.14	-0.14	**-0.28**	**0.53**	**-0.34**	0.19	0.17	-0.03	**-0.46**	-0.24	-0.19	**-0.31**	**0.33**	**0.61**	**0.38**	**0.43**
$\%F_{C1}$	**-0.66**	**-0.21**	**0.64**	**-0.79**	**0.18**	**0.69**		**-0.73**	**0.46**	**-0.65**	**-0.76**	**0.43**	0.18	-0.15	-0.19	0.02	**-0.34**	**-0.40**	-0.21	0.08	**0.42**	0.19	**0.48**	0.27
$\%F_{C2}$	**0.70**	0.13	**-0.81**	**0.73**	-0.07	**-0.25**	**-0.73**		**-0.84**	**0.75**	**0.95**	**-0.40**	-0.22	0.08	**0.32**	-0.09	0.07	0.30	0.15	-0.07	-0.24	0.03	-0.26	0.00
$\%F_{C3}$	**-0.53**	**-0.18**	**0.64**	**-0.53**	-0.06	-0.14	**0.46**	**-0.84**		**-0.73**	**-0.81**	0.13	0.29	-0.17	-0.26	0.07	0.01	-0.21	-0.12	0.17	0.14	-0.18	0.19	-0.06
$\%F_{C4}$	**0.36**	**0.19**	**-0.61**	**0.56**	**-0.16**	-0.14	**-0.65**	**0.75**	**-0.73**		**0.84**	-0.10	-0.17	0.18	0.11	-0.07	0.08	0.24	0.24	-0.21	-0.21	0.11	**-0.33**	-0.10
$\%F_{C5}$	**0.66**	0.10	**-0.78**	**0.71**	-0.13	**-0.28**	**-0.76**	**0.95**	**-0.81**	**0.84**		**-0.37**	-0.14	0.05	0.30	-0.21	0.08	0.29	0.19	0.01	-0.26	0.02	-0.28	-0.01
DOC	**-0.71**	**0.29**	**0.36**	**-0.37**	**0.35**	**0.53**	**0.43**	**-0.40**	0.13	-0.10	**-0.37**		-0.16	0.07	0.03	0.03	**-0.33**	**-0.39**	-0.27	-0.22	**0.38**	**0.43**	**0.43**	**0.40**
% CHO	**-0.41**	0.11	0.22	**-0.34**	-0.11	**-0.34**	0.18	-0.22	0.29	-0.17	-0.14	-0.16		**-0.84**	-0.30	**-0.42**	0.20	-0.24	-0.11	**0.58**	0.01	**-0.44**	-0.12	-0.13
% CHOS	**0.33**	-0.23	-0.07	0.26	0.16	0.19	-0.15	0.08	-0.17	0.18	0.05	0.07	**-0.84**		-0.18	**0.63**	0.07	**0.35**	0.30	**-0.55**	-0.26	0.25	-0.05	-0.22
% CHON	0.26	0.22	**-0.36**	0.20	0.15	0.17	-0.19	**0.32**	-0.26	0.11	0.30	0.03	-0.30	-0.18		**-0.52**	**-0.37**	0.14	0.04	-0.03	0.16	0.26	0.08	**0.50**
% CHONS	0.05	-0.13	0.08	0.02	0.00	-0.03	0.02	-0.09	0.07	-0.07	-0.21	0.03	**-0.42**	**0.63**	**-0.52**		0.23	0.03	-0.07	**-0.43**	-0.11	-0.09	0.07	**-0.31**
% Lipid	0.11	0.05	-0.06	0.17	0.16	**-0.46**	**-0.34**	0.07	0.01	0.08	0.08	**-0.33**	0.20	0.07	**-0.37**	0.23		**0.36**	0.02	-0.11	**-0.71**	**-0.77**	**-0.78**	**-0.87**
% Protein	**0.41**	0.13	**-0.38**	**0.35**	**0.42**	-0.24	**-0.40**	0.30	-0.21	0.24	0.29	**-0.39**	-0.24	**0.35**	0.14	0.03	**0.36**		**0.76**	-0.07	**-0.82**	-0.27	**-0.52**	**-0.56**
% Carb	0.22	0.10	-0.23	0.17	**0.40**	-0.19	-0.21	0.15	-0.12	0.24	0.19	-0.27	-0.11	0.30	0.04	-0.07	0.02	**0.76**		-0.06	**-0.48**	-0.03	**-0.33**	**-0.32**
% UHC	-0.25	-0.07	0.03	-0.13	-0.02	**-0.31**	0.08	-0.07	0.17	-0.21	0.01	-0.22	**0.58**	**-0.55**	-0.03	**-0.43**	-0.11	-0.07	-0.06		0.08	-0.30	0.27	0.10
% Lignin	**-0.35**	-0.20	**0.32**	-0.26	**-0.46**	**0.33**	**0.42**	-0.24	0.14	-0.21	-0.26	**0.38**	0.01	-0.26	0.16	-0.11	**-0.71**	**-0.82**	**-0.48**	0.08		**0.44**	**0.72**	**0.74**
% CAS	0.17	0.12	-0.06	-0.01	-0.12	**0.61**	0.19	0.03	-0.18	0.11	0.02	**0.43**	**-0.44**	0.25	0.26	-0.09	**-0.77**	-0.27	-0.03	-0.30	**0.44**		**0.53**	**0.75**
DBE	-0.29	-0.15	0.20	-0.28	-0.25	**0.38**	**0.48**	-0.26	0.19	**-0.33**	-0.28	**0.43**	-0.12	-0.05	0.08	0.07	**-0.78**	**-0.52**	**-0.33**	0.27	**0.72**	**0.53**		**0.76**
AI_{mod}	-0.05	0.17	-0.08	-0.14	-0.08	**0.43**	0.27	0.00	-0.06	-0.10	-0.01	**0.40**	-0.13	-0.22	**0.50**	**-0.31**	**-0.87**	**-0.56**	**-0.32**	0.10	**0.74**	**0.75**	**0.76**	

% CHO formulas is positively correlated with % unsaturated hydrocarbon-like formulas and negatively correlated with $SUVA_{255}$ and % condensed aromatic ring structure formulas (Table 6). The majority of formulas come from the CHO series for all samples, with CHO formulas comprising 58.0 % to 77.6 % of total formulas among samples (Table 7). The CHO series has been repeatedly found to be the most common series in streams and rivers in previous studies (Lu et al., 2015b). The other series making up the rest of the formulas, in the order of prevalence, include CHON (15.5-25.5 %), CHOS (4.7-19.8 %), and CHONS (0.2-2.0 %). Lake samples are statistically lower in CHO formulas compared to Main and Tributary samples. Tributary samples are statistically lower in CHON formulas compared to Lake samples.

Table 7: Percent of formulas belonging to each series. Significantly different pairs based on Dunn's test are indicated by different letters following the average.

Sample	% CHO	% CHOS	% CHON	% CHONS
A2	69.3	10.9	19.6	0.2
A5	73.1	8.5	18.0	0.4
A10	71.0	6.7	22.1	0.2
A13	74.6	5.5	19.7	0.3
A15	75.3	4.7	19.8	0.2
A20	62.2	19.8	16.9	1.0
B2	75.4	5.1	19.2	0.3
B7	77.6	5.8	15.5	1.0
B12	69.3	8.8	21.5	0.4
B14	66.7	15.0	16.2	2.0
B17	61.8	17.6	19.9	0.7
B20	63.7	15.5	20.2	0.6
B21	72.7	7.8	19.2	0.3
G1	68.2	6.2	25.1	0.4
L2	60.6	17.6	21.2	0.6
L4	61.8	19.3	18.1	0.8
L5	57.3	15.7	25.5	1.5
L6	63.7	13.5	21.6	1.2
L10	61.0	13.2	25.4	0.3
L11	63.2	14.1	22.5	0.2
L12	58.0	17.3	23.6	1.0
Average				
Main	70.9 (a)	9.4 (a)	19.4 (ab)	0.4 (a)
Tributary	69.6 (a)	10.8 (a)	18.8 (a)	0.8 (a)
Lake	60.8 (b)	15.8 (a)	22.6 (b)	0.8 (a)

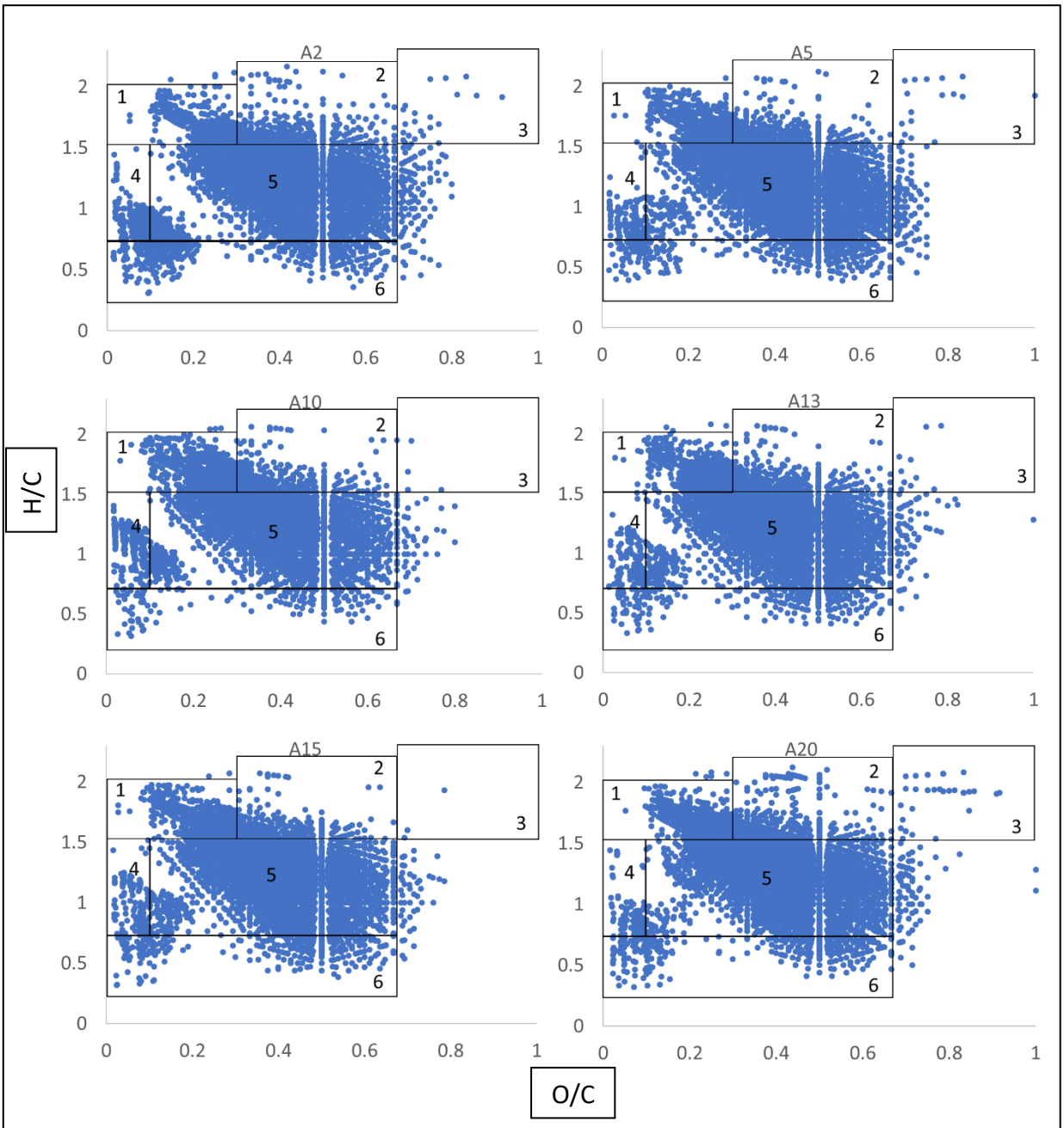

Figure 9: Van Krevelen diagrams of Main samples. Numbers correspond to biochemical classes: (1) lipid-like, (2) protein -like, (3) carbohydrate-like, (4) unsaturated hydrocarbon-like, (5) lignin-like, and (6) condensed aromatic ring structure.

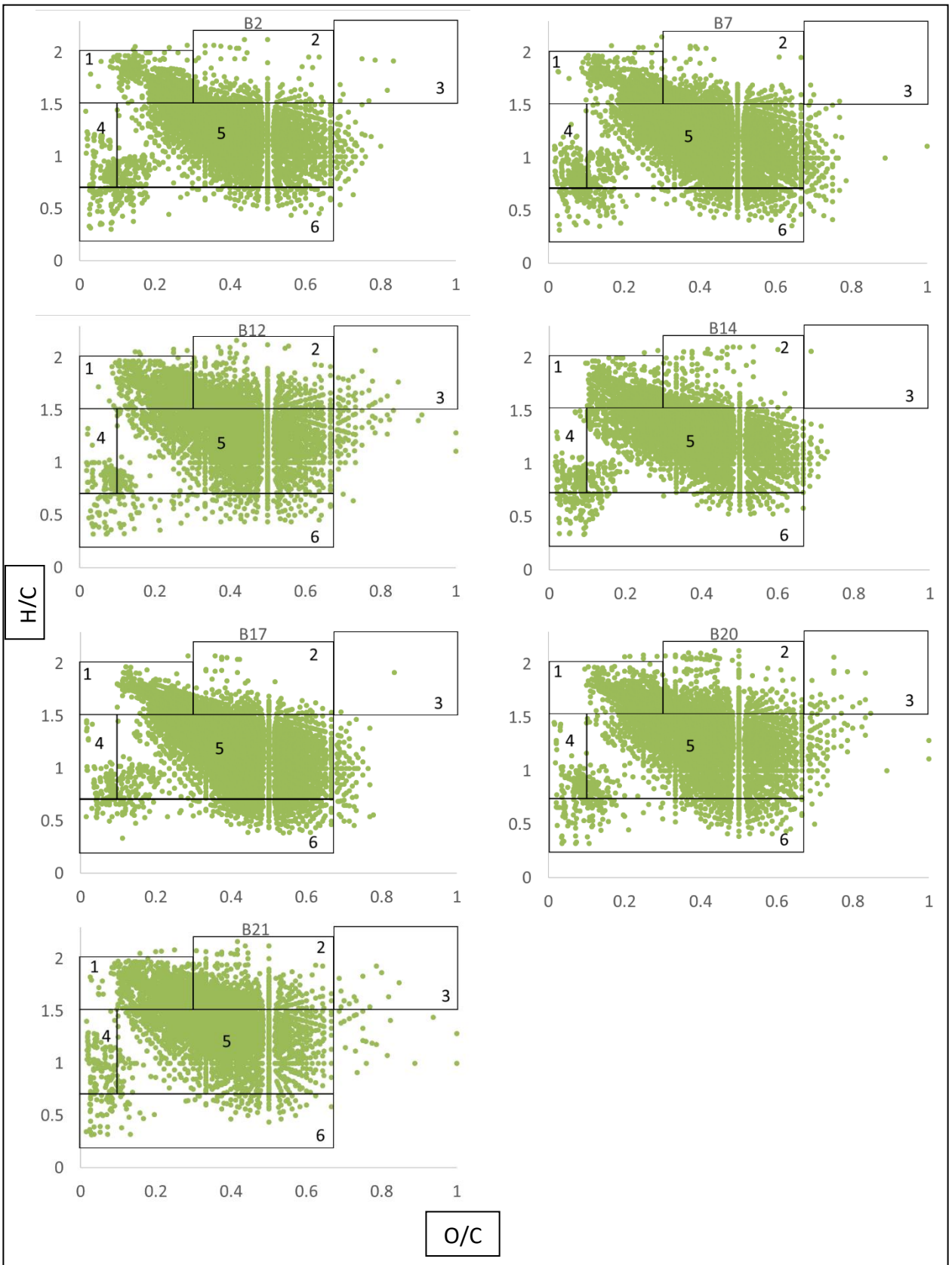

Figure 10: Van Krevelen Diagrams of Tributary samples. Numbers correspond to biochemical classes: (1) lipid-like, (2) protein-like, (3) carbohydrate-like, (4) unsaturated hydrocarbon-like, (5) lignin-like, and (6) condensed aromatic ring structure.

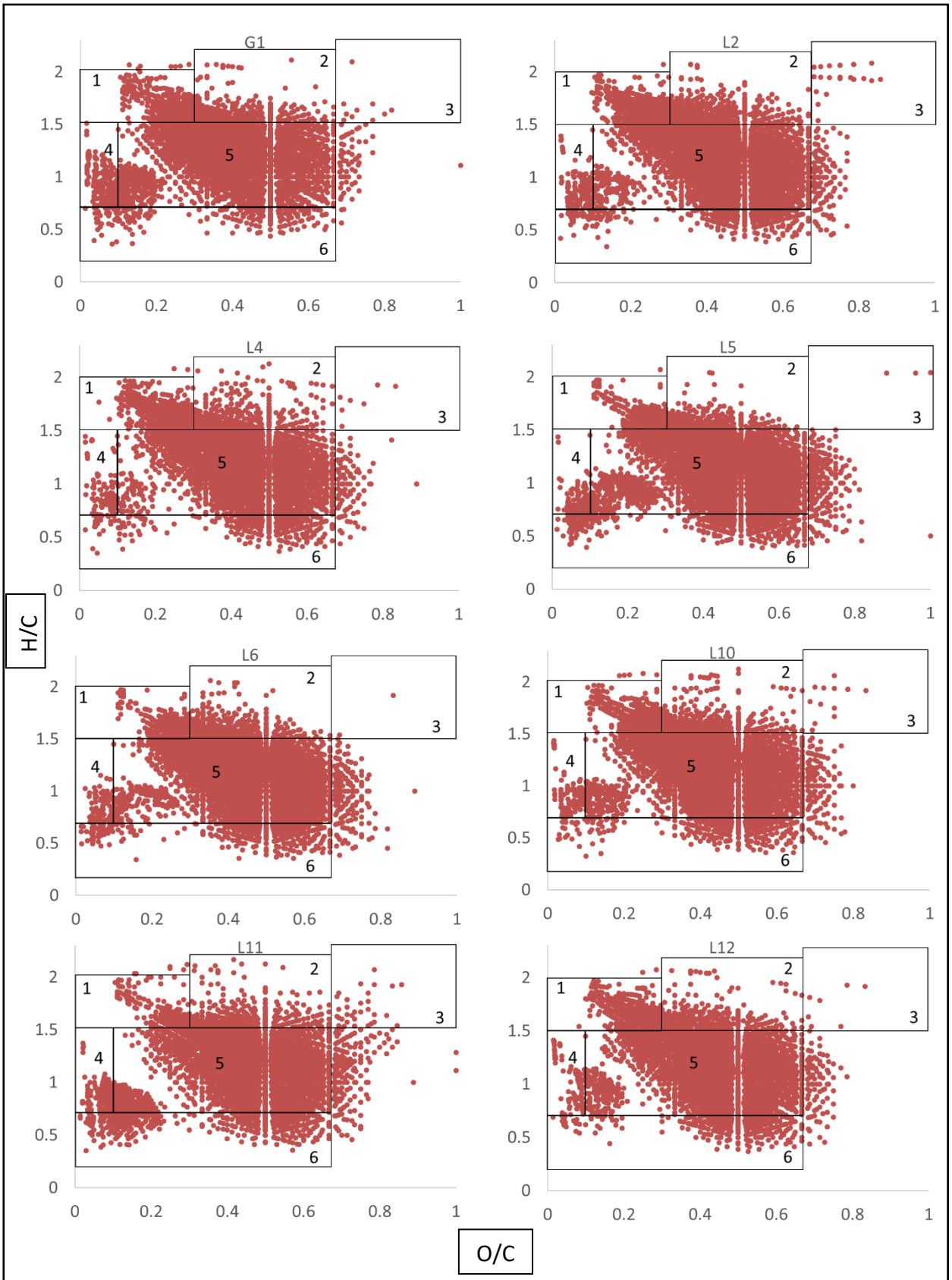

Figure 11: Van Krevelen Diagrams of Lake samples. Numbers correspond to biochemical classes: (1) lipid-like, (2) protein-like, (3) carbohydrate-like, (4) unsaturated hydrocarbon-like, (5) lignin-like, and (6) condensed aromatic ring structure.

Van Krevelen diagrams were constructed for all samples using their H/C and O/C atomic ratios. Six regions on the Van Krevelen diagrams correspond to the following six biochemical classes: (1) lipid-like (H/C=1.5-2.0, O/C=0-0.3), (2) protein-like (H/C=1.5-2.2, O/C=0.3-0.67), (3) carbohydrate-like (H/C=1.5-2.4, O/C=0.67-1.2), (4) unsaturated hydrocarbon-like (H/C=0.7-1.5, O/C=0-0.1), (5) lignin-like (H/C=0.7-1.5, O/C=0.1-0.67), and (6) condensed aromatic ring structure (H/C=0.2-0.7, O/C=0-0.67) (Figure 7, 8, & 9) (Hockaday et al. 2009, Oh no et al., 2010; Lu et al., 2015b). Based on H/C and O/C ratios, lignin-like formulas dominate (56.6-77.7 %) in all samples followed by lipid-like (5.5-21.5 %) and protein-like (6.6-19.0 %) formulas, with the other three classes making up minor portions (Table 8). Tributary and Lake samples are statistically different from each other in percentage of lipid-like, 15.4 % and 9.7 %, respectively, and condensed aromatic ring structure, 4.3 % and 6.4 %, respectively, formulas while Main samples are not statistically different from either.

Table 8: Percent of formulas belonging to six biochemical classes based on H/C and O/C ratios. Significantly different pairs based on Dunn's test are indicated by different letters following the average.

Sample	% Lipid-like	% Protein-like	% Carbohydrate-like	% Unsaturated Hydrocarbon-like	% Lignin-like	% Condensed aromatic ring structure
A2	10.4	9.7	0.6	4.1	69.7	6.5
A5	11.9	8.9	0.4	2.7	71.7	5.6
A10	16.6	9.3	0.1	5.1	67.3	3.4
A13	12.7	9.2	0.3	2.7	71.5	4.9
A15	13.9	8.5	0.1	2.7	71.7	4.7
A20	14.8	10.0	0.7	2.4	68.9	4.6
B2	12.7	7.4	0.2	2.6	73.9	4.0
B7	12.6	8.0	0.1	2.9	71.4	5.4
B12	17.8	17.4	0.9	1.9	60.0	4.0
B14	16.3	7.8	0.0	3.2	72.3	2.7
B17	11.3	6.9	0.0	1.7	74.2	7.1
B20	15.6	14.8	0.6	2.4	64.2	4.4
B21	21.5	19.0	0.4	2.8	56.6	2.8
G1	10.4	9.5	0.3	5.0	71.8	4.3
L2	12.4	10.2	0.4	2.5	70.1	5.5
L4	14.9	9.2	0.1	1.7	69.5	5.8
L5	6.3	6.6	0.1	1.9	77.6	6.7
L6	6.1	8.2	0.0	1.5	77.7	6.4
L10	9.4	8.9	0.2	2.0	72.9	7.0
L11	5.5	9.3	0.8	3.3	72.6	8.4
L12	12.4	9.4	0.2	2.2	70.4	6.8
Average						
Main	13.4 (ab)	9.3 (a)	0.4 (a)	3.3 (a)	70.1 (a)	4.9 (ab)
Tributary	15.4 (a)	11.6 (a)	0.3 (a)	2.5 (a)	67.5 (a)	4.3 (a)
Lake	9.7(b)	8.9 (a)	0.3 (a)	2.5 (a)	72.8 (a)	6.4 (b)

Average formula atomic numbers, H/C and O/C ratios, double bond equivalents and molecular weight are not statistically different among sample groupings (Table 9). The average H/C and O/C ratios for all samples fall within the lignin-like range. AI_{mod} values >0.67 are considered condensed aromatic structures, 0.5 to 0.67 are considered aromatic, and <0.5 are considered aliphatic and olefinic compounds (Stubbins et al., 2014; Lu et al., 2015). Average AI_{mod} values for all samples, fall within the aliphatic and olefinic compound range. AI_{mod} values are statistically higher for Lake samples, averaging 0.30, compared to Tributary samples, averaging 0.26, while that of Main samples are not statistically different from either.

Table 9: Average formula atomic numbers, O/C and H/C ratios, Double Bond Equivalents (DBE), molecular weight (m/z), and modified aromaticity index (AI_{mod}). AI_{mod} values are significant based on Kruskal-Wallis test ($P<0.05$). Significantly different pairs based on Dunn's test are indicated by different letters following the average.

Sample	C	H	O	H/C	O/C	DBE (n)	m/z	AI_{mod}
A2	26.9	32.9	9.5	1.2	0.4	11.1	515.2	0.29
A5	28.0	34.6	10.1	1.2	0.4	11.3	537.7	0.29
A10	27.2	35.0	8.6	1.3	0.4	10.3	505.2	0.28
A13	27.3	34.6	9.6	1.2	0.4	9.6	520.5	0.28
A15	27.9	35.6	9.7	1.2	0.4	10.8	530.6	0.29
A20	27.8	35.7	9.8	1.3	0.4	10.6	536.2	0.26
B2	27.5	34.8	9.7	1.2	0.4	10.7	525.9	0.28
B7	28.8	35.8	10.2	1.2	0.4	11.5	549.3	0.29
B12	24.4	33.3	8.6	1.3	0.4	8.4	470.3	0.26
B14	29.9	38.8	9.6	1.3	0.3	11.1	560.2	0.26
B17	27.5	33.5	10.3	1.2	0.4	11.4	538.1	0.31
B20	26.2	34.6	9.3	1.3	0.4	9.5	506.1	0.24
B21	26.2	36.7	8.3	1.4	0.3	8.5	491.1	0.21
G1	28.1	34.2	9.2	1.2	0.4	11.6	525.1	0.30
L2	28.0	34.7	10.2	1.2	0.4	11.3	544.5	0.28
L4	27.4	34.7	9.9	1.2	0.4	10.7	532.3	0.28
L5	29.6	34.5	11.3	1.2	0.4	13.0	581.1	0.31
L6	28.1	33.5	11.2	1.2	0.4	12.0	558.9	0.30
L10	26.1	31.5	9.8	1.2	0.4	11.0	511.2	0.31
L11	25.5	29.6	9.9	1.2	0.4	11.4	503.0	0.32
L12	26.6	32.6	9.7	1.2	0.4	10.9	516.1	0.30
Average								
Main	27.5 (a)	34.7 (a)	9.5 (a)	0.4 (a)	1.2 (a)	10.6 (a)	524.2 (a)	0.28 (ab)
Tributary	27.2 (a)	35.4 (a)	9.4 (a)	0.4 (a)	1.3 (a)	10.2 (a)	520.2 (a)	0.26 (a)
Lake	27.4 (a)	33.2 (a)	10.2 (a)	0.4 (a)	1.2 (a)	11.5 (a)	534.0 (a)	0.30 (b)

Unsurprisingly, with the average AI_{mod} value for all samples < 0.5, the majority of compounds have an AI_{mod} value < 0.5 (Table 10). Approximately 75-90 % of compounds fall within this aliphatic and olefinic range. The average number of compounds belonging to the upper two ranges—AI_{mod} > 0.67 and AI_{mod} 0.5-0.67—significantly differs between Lake and Tributary samples. Lake samples have more compounds falling in these upper two ranges compared to Tributary samples.

Table 10: Number of compounds falling within each AI_{mod} range. Values are significant for two AI_{mod} ranges based on Kruskal-Wallis test ($P<0.05$). Significantly different pairs based on Dunn's test are indicated by different letters.

Sample	AI > 0.67	AI 0.5-0.67	AI < 0.5
A2	225	733	3925
A5	207	697	4482
A10	91	463	3309
A13	162	601	3930
A15	163	590	4042
A20	160	554	4356
B2	127	500	3641
B7	177	653	4224
B12	140	386	3685
B14	98	416	4044
B17	233	892	4604
B20	156	533	4166
B21	91	312	3726
G1	133	763	3686
L2	205	824	4859
L4	181	666	4441
L5	289	1037	5517
L6	271	897	5291
L10	248	891	4227
L11	277	924	3801
L12	181	776	3832
Average			
Main	168 (ab)	606 (ab)	4007 (a)
Tributary	146 (a)	527 (a)	4013 (a)
Lake	223 (b)	847 (b)	4457 (a)

Incubation Results

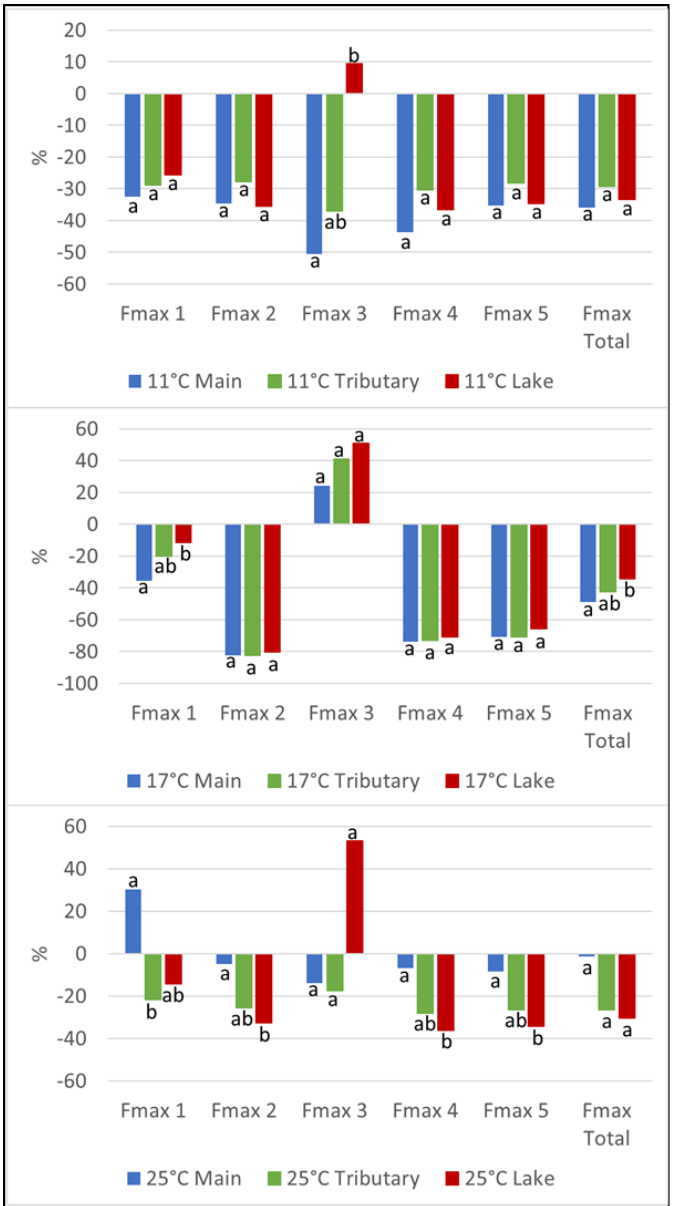

Figure 12: Average percent change in maximum fluorescence (Fmax) over 5-day incubation period (T0 to T5) for main, tributary, and lake samples at temperatures 11°C, 17°C, and 25°C. Fmax 1 corresponds to Component 1, Fmax 2 to Component 2, etc. Fmax Total is the sum of all 5 fluorescence components. Based on Dunn's test, significantly different percent changes between main, tributary, and lake samples for each Fmax are indicated by different letters.

The incubation fluorescence data has been incorporated into the 5-component model created with the Parlung Zangbo main stem river, tributary, and lake water samples (Figure 4). The percent change in fluorescence from the start of incubation (T0) to the end of incubation (T5) has been calculated for each sample using the model output maximum fluorescence (Fmax), with each component having a corresponding Fmax, e.g., C1 corresponds to Fmax 1 (Figure 12). For the experiment conducted at 11°C, percent change in fluorescence is not statistically different among Main, Tributary, and Lake samples for all components, excluding C3. The decrease in C3 for Main samples (-50.6 %) is statistically different from the increase (+9.4 %) in Lake samples. This trend of greater increase in Lake samples compared to Main samples for C3 is observed in experiments at 17°C and 25°C as well, yet it is not statistically significant for these two experiments. C3 is associated with DOM produced through biodegradation, explaining its increase during incubation. For the experiment conducted at 17°C, percent change in fluorescence in C1 is statistically different between Main and Lake samples with greatest decrease in Main samples (-35.5 %) and smallest decrease in Lake samples (-11.3 %). The same relationship is observed in percent change in total fluorescence at 17°C with greatest decrease in Main samples (-48.9 %) and smallest decrease in Lake samples (-34.2 %). For the experiment conducted at 25°C, percent change in fluorescence in C2, C4, and C5 is statistically different between Main and Lake samples with greatest decrease observed in Lake samples and smallest decrease in Main samples. In C1, an increase is observed in Main samples, but the greatest decrease is observed in Tributary samples rather than Lake samples. C1 is composed of humic-like compounds that are potentially OM degradation products which may explain the increase in C1. The change in total fluorescence at 25°C was not statistically different among sample groupings. Figures 13 and 14 compare percent change in fluorescence among 11°C, 17°C, and

25°C experiments. Comparing averages for all samples of each experiment, the percent change in total fluorescence (Fmax Total) the 17°C experiment has the greatest decrease (-43.0 %), and the 25°C experiment has the smallest decrease (-16.5 %), though it is statistically similar to that of the 11°C experiment (-33.0 %) (Figure 13). Percent change in total fluorescence in Main samples follows the same trend with the greatest decrease observed in Main 17°C samples (-48.9 %), and the smallest decrease is observed in Main 25°C samples (-1.3 %), which is statistically similar to Main 11°C samples (-36.0 %) (Figure 14). For Tributary samples, the 17°C experiment has the greatest decrease in total fluorescence. Percent change in total fluorescence in Lake samples is not statistically different among the 11°C, 17°C, and 25°C experiments.

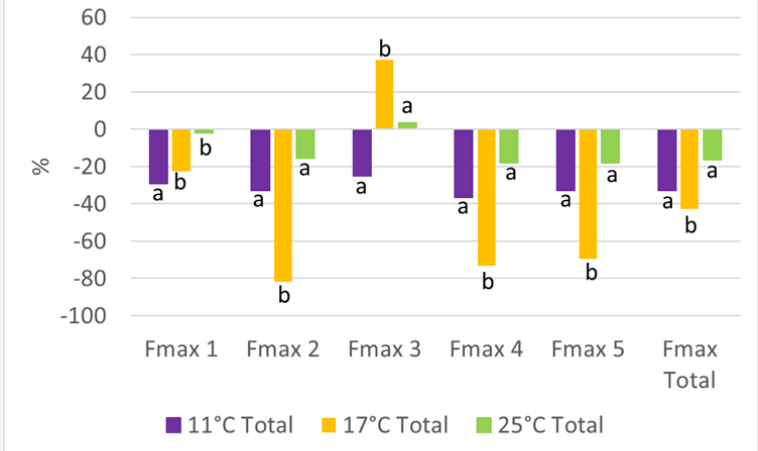

Figure 13: Average percent change in maximum fluorescence (Fmax) over 5-day incubation period (T0 to T5) for all samples at temperatures 11°C, 17°C, and 25°C. Fmax 1 corresponds to Component 1, Fmax 2 to Component 2, etc. Fmax Total is the sum of all 5 fluorescence components. Based on Dunn's test, significantly different percent changes between 11°C, 17°C, and 25°C samples for each Fmax are indicated by different letters.

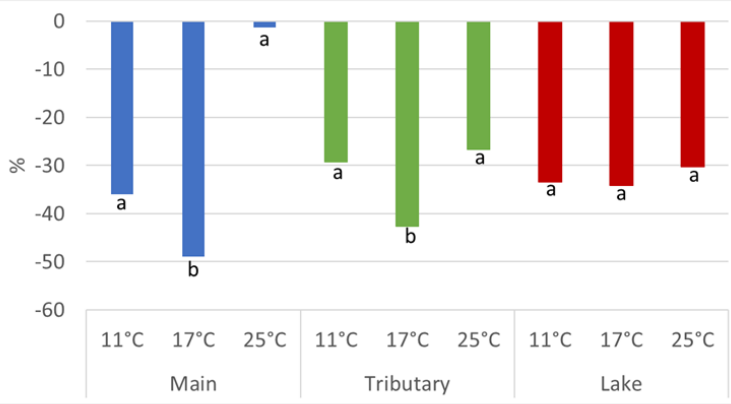

Figure 14: Average percent change in maximum Fmax Total over 5-day incubation period (T0 to T5) for Main, Tributary, and Lake samples at temperatures 11°C, 17°C, and 25°C. Fmax Total is the sum of all 5 fluorescence components. Based on Dunn's test, significantly different percent changes between 11°C, 17°C, and 25°C samples for Fmax Total are indicated by different letters.

Unexpectedly, DOC increased in some samples in the over the 5-day incubation period (Figures 15 & 16). DOC concentrations have been observed to remain relatively unchanged in similar amounts of time (3-5 days) in incubation experiments in previous studies (Hansen et al., 2016; Shang et al., 2018). The bacterial inoculate was filtered before being added to the samples, so no particulate organic matter would be expected. However, since DOC concentrations actually increased some samples in these experiments, this may mean samples were contaminated or the bacterial inoculate may have contained particulate organic matter which acted as a source for DOC during the incubation. Increases in DOC concentration proprogated unexpected results in absorbance indices, too. $SUVA_{255}$ would be expected to increase as lower molecular weight, aliphatic DOM is biodegradaed first; however, $SUVA_{255}$ decreased in experiments at each temperature. Contradictory to $SUVA_{255}$, S_R decreased in 11°C and 25°C experiments and Lake samples of the 17°C experiment. E2:E3 increased for all experiments suggesting decrease in the average molecular size of the DOM pool. FI values decreased for all experiments; FI values were expected to increase during incubation as microbial processing of labile DOM produces a greater portion of microbially-dervied DOM. Additionally, B:α decreased in all experiments suggesting the DOM pool became less fresh and more humic-like. HIX values increased for all groupings of the 11°C and 25°C experiment and Main samples of the 17°C experiment, which suggests increased humification of the DOM pool as well.

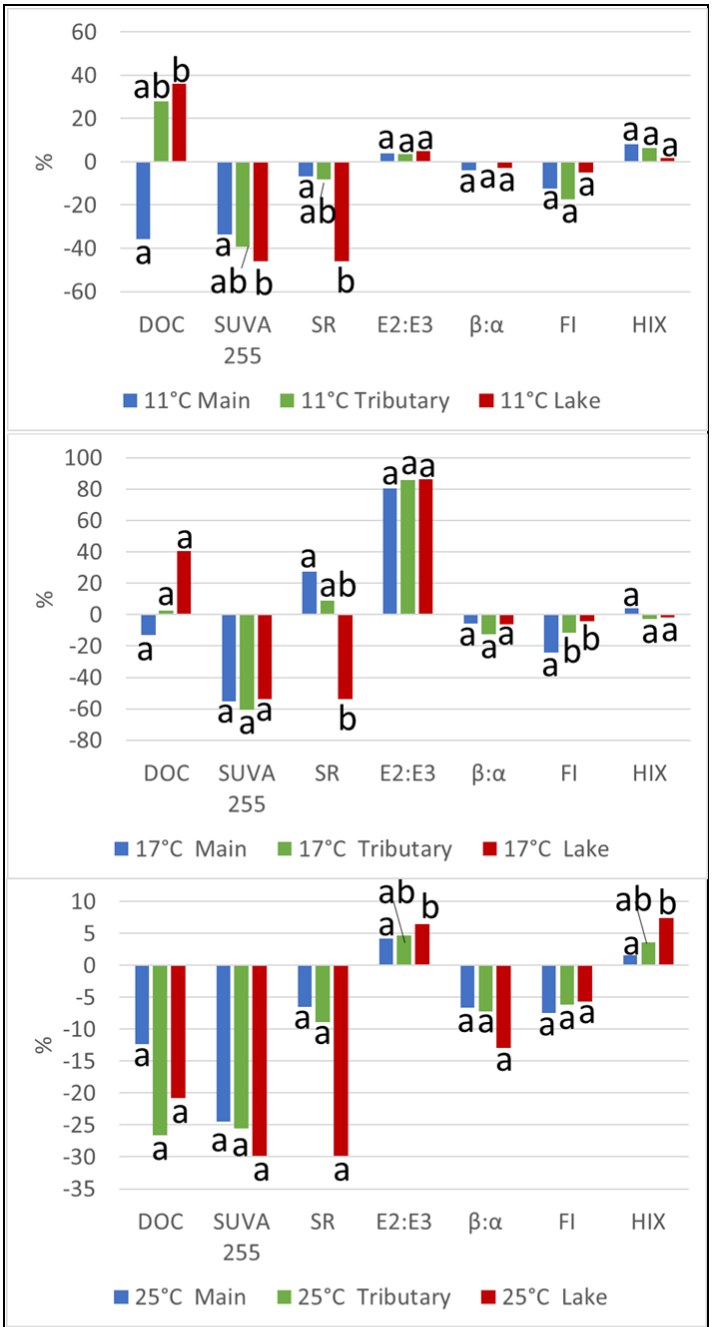

Figure 15: Average percent change in DOC, SUVA255, SR, E2:E3, β:α, FI, and HIX over 5-day incubation period (T0 to T5) for main, tributary, and lake samples at temperatures 11°C, 17°C, and 25°C. Based on Dunn's test, significantly different percent changes between main, tributary, and lake samples for each are indicated by different letters.

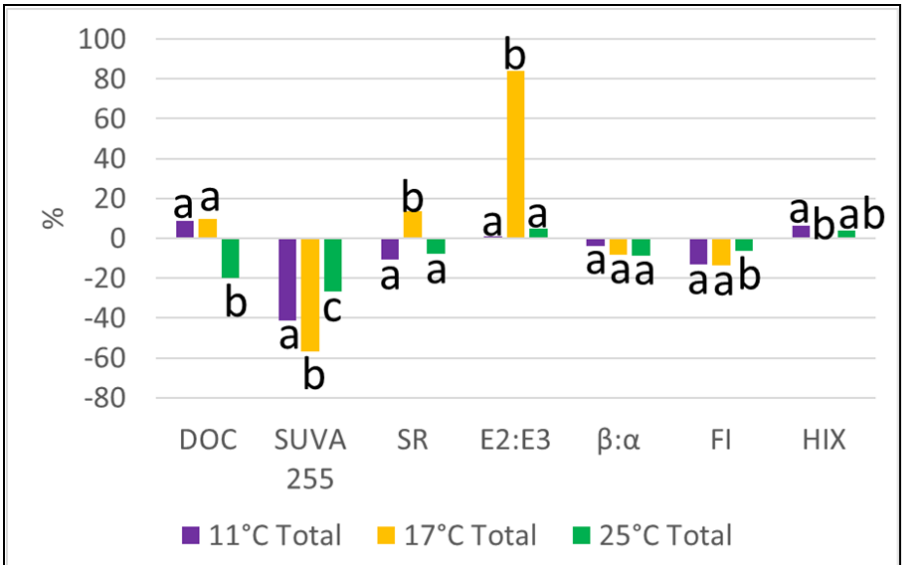

Figure 16: Average percent change in DOC, SUVA255, SR, E2:E3, β:α FI, and HIX over 5-day incubation period (T0 to T5) for all samples at temperatures 11°C, 17°C, and 25°C. Based on Dunn's test, significantly different percent changes between 11°C, 17°C, and 25°C samples for each are indicated by different letters.

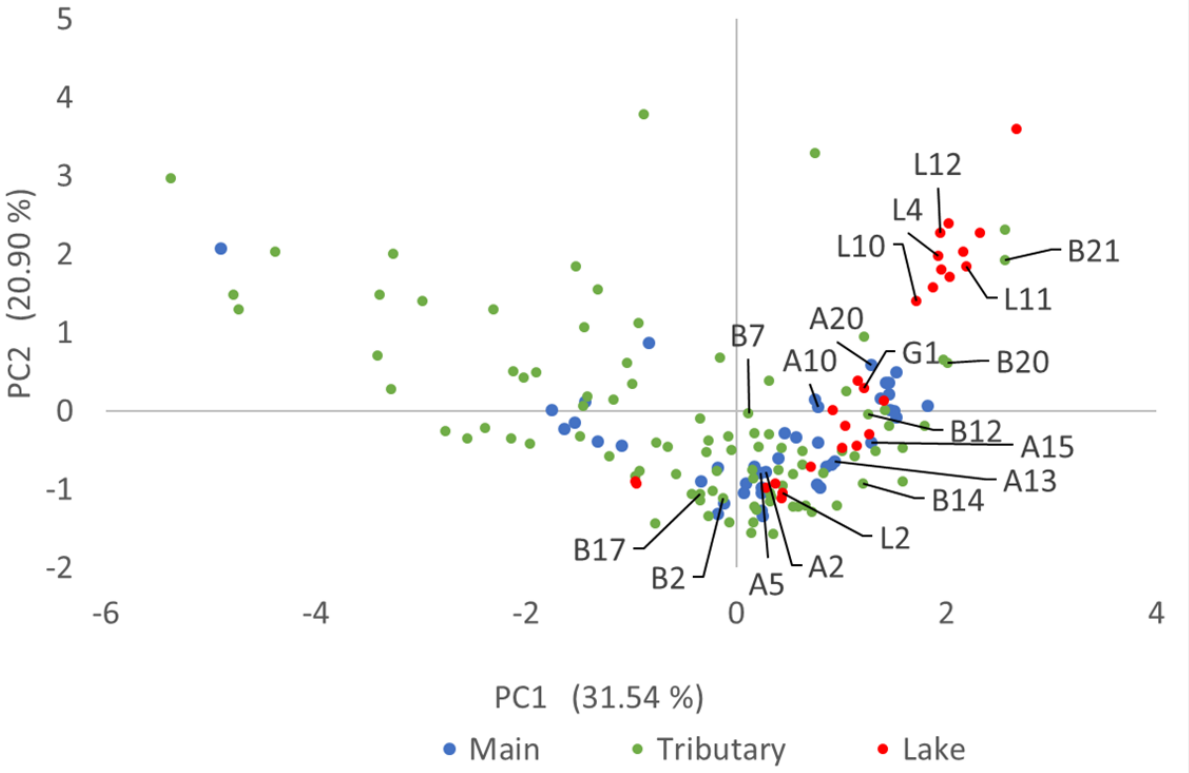

Figure 17: Parlung Zangbo River samples plotted with PC1 (31.54%) and PC2 (20.90%) from PCA showing 52.44% of total variance. Sample groupings indicated by color, i.e., Main-blue, Tributary-green, and Lake-red. The following variables were included in the PCA: $SUVA_{255}$, S_R, HIX, FI, β:α, Fmax1, Fmax 3, and DOC. Samples analyzed with FT-ICR-MS are labeled.

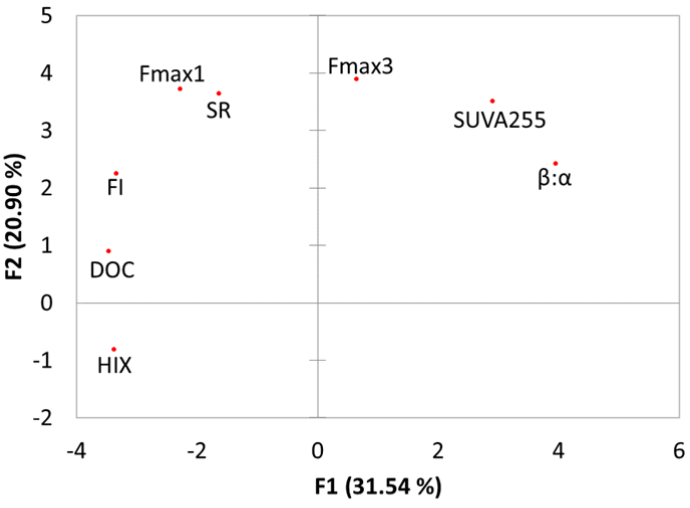

Figure 18: Variable loadings of principal components 1 and 2 from PCA in Figure 17.

PCA was performed with data from the original 179 samples from along the Parlung Zangbo main stem, nearby tributaries, and headwater lake. Variables included in the PCA were selected based on sampling adequacy and multicollinearity tests, and selected variables include $SUVA_{255}$, S_R, HIX, FI, β:α, Fmax1, Fmax3, and DOC. The first two principal components (PC1 & PC2) from PCA capture 52.44% of total variance among all samples and are used as axes to plot the samples (Figure 17). Plotting the PCA results reveals overlap between sampling groupings: Main, Tributary, and Lake. While plotting the samples does not expose distinct groups, Lake samples are noticeably congregated in the right upper quadrant, and Tributary samples are the most variable. Main samples mostly fall within the extremes of Lake and Tributary samples. The two tributary samples that plot in the right upper quadrant with the Lake samples are from tributaries nearby the lake, thus these samples' compositional similarity is coincident with spatial proximity to the lake. DOC and HIX negatively control PC1 (Figure18). Fmax3, S_R, and Fmax1 positively control PC2. $SUVA_{255}$ and β:α positively controls PC1 &PC2. Low DOC concentrations and higher B:α are characteristics of Lake samples that correspond to plotting in the upper right quadrant.

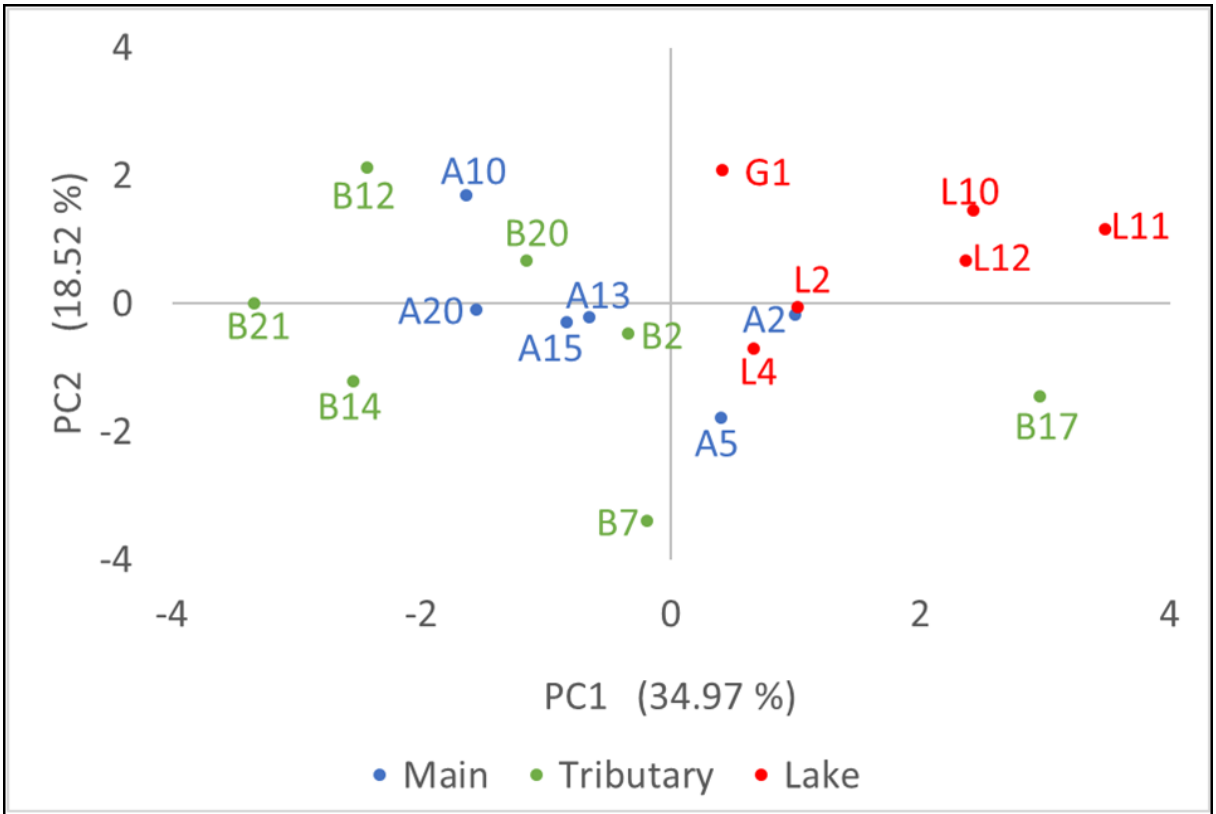

Figure 19: Samples analyzed with FT-ICR-MS data plotted with PC1 (34.97%) and PC2 (18.52%) from PCA showing 53.49% of total variance. The following variables were included in the PCA: S_R, HIX, FI, DOC, Fmax3, %CHO, %CHON, %Lipid, %CAS, and AI_{mod}.

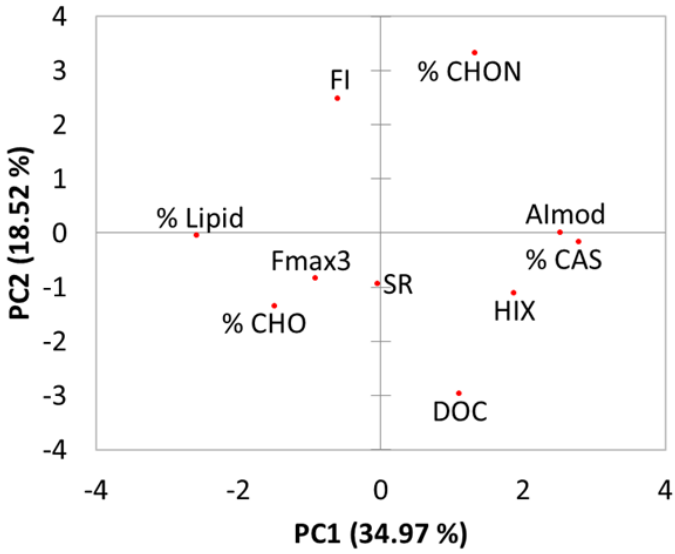

Figure 20: Variable loadings of principal components 1 and 2 from PCA in Figure 19.

The same pattern observed in Figure 17 can be seen in Figure 19 which is created with the addition of FT-ICR-MS data for the subset of 21 samples for which this data is available. Variables included in this PCA were selected with the same criteria for sampling adequacy and multicollinearity, and selected variables include S_R, HIX, FI, DOC, Fmax3, %CHO, %CHON, %Lipid, %CAS, and AI_{mod}. This distribution of samples seen in Figure 17 & 19 can be interpreted to show the headwater lake and tributaries contribute to the main stem river creating Main samples that are intermediate in composition between Lake and Tributary samples. AI_{mod} and %CAS strongly positively control PC1; HIX also positively controls PC1 (Figure 19). %Lipid strongly negatively controls PC1. S_R strongly negatively controls PC2; DOC and HIX also negatively control PC2. FI and %CHON positively control PC2. Fmax3 and %CHO negatively control PC1 & PC2. Low DOC, higher AI_{mod}, %CAS, %CHON are characteristics of Lake samples that correspond to plotting in the upper right quadrant.

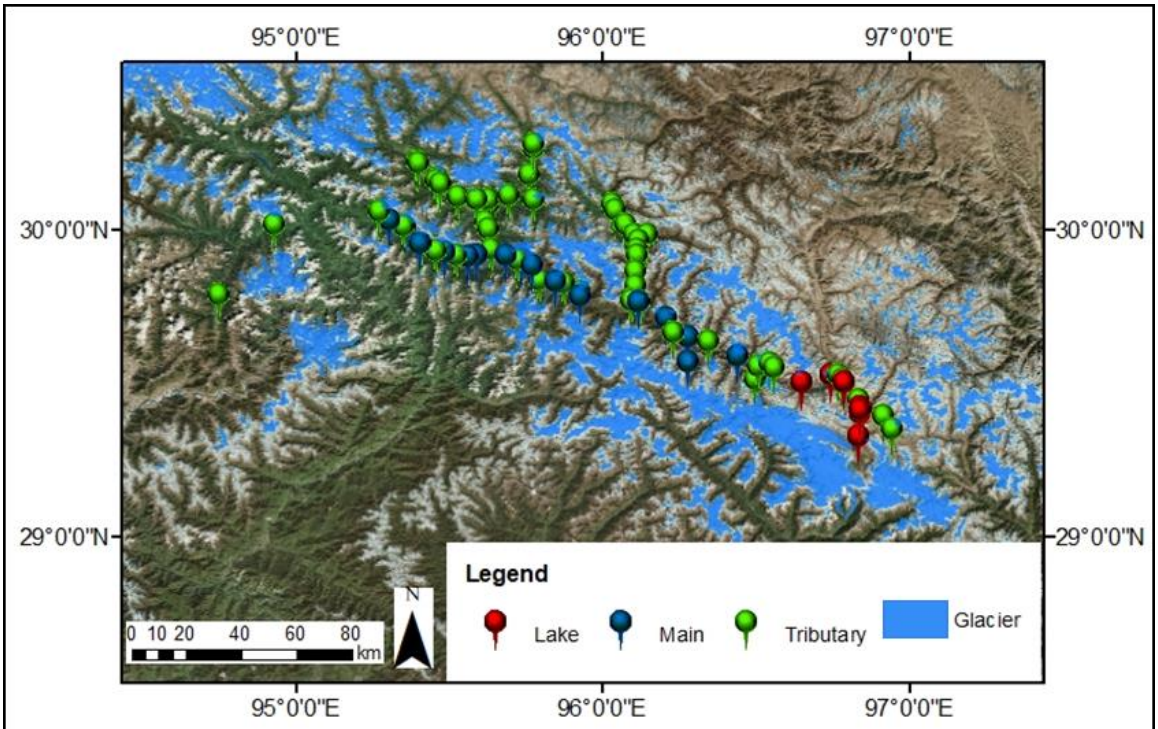

Figure 21: Map of sampling sites showing glacial coverage. Map created with ArcGIS; glacier data from GLIMS Randolph Glacier Inventory (2016).

Generally, Lake samples are characterized by low DOC, higher proportions of C2 (soluble microbial byproduct-like), have a higher proportion of fresh DOM (β:α), higher %CHON, and higher AI_{mod}. A study on seasonal DOM variation in a glacial environment by Barker et al. (2009) finds microbial DOM is flushed from snowpack and dominates in supraglacial meltwater. The proximity of the Lake to glacier suggests the source of C2 is likely supraglacial meltwater, too (Figure 21). Additionally, glacial melt has been associated with higher N levels which is consistent with higher %CHON in Lake samples (Hood and Berner, 2009; Fountain et al., 2012; Milner et al., 2017). Lake samples are more enriched in aromatic compounds, higher AI_{mod}, which is an expected signature of permafrost. Tributary samples are the most variable group, have the highest DOC concentrations, and have the higher proportions of C3 (tryptophan-like) relative to Lake samples. Data from NOAA show much of the region has sporadic permafrost cover ranging from 10 – 50 % (Figure 22). The permafrost data shows permafrost exists over much of the area where Tributary and Lake samples were collected; however, whether Tributary or Lake samples come from areas of greater permafrost coverage relative to each other is unclear because the data does not provide greater resolution than 10 – 50 % coverage. C3 represents a tryptophan-like component of DOM which is associated with autochthonous production of DOM through biodegradation (Dubnick et al., 2010). The dominance of autochthonous DOM is supported by an average HIX value of 0.49, an indicator of autochthonous DOM (Huguet et al., 2009).

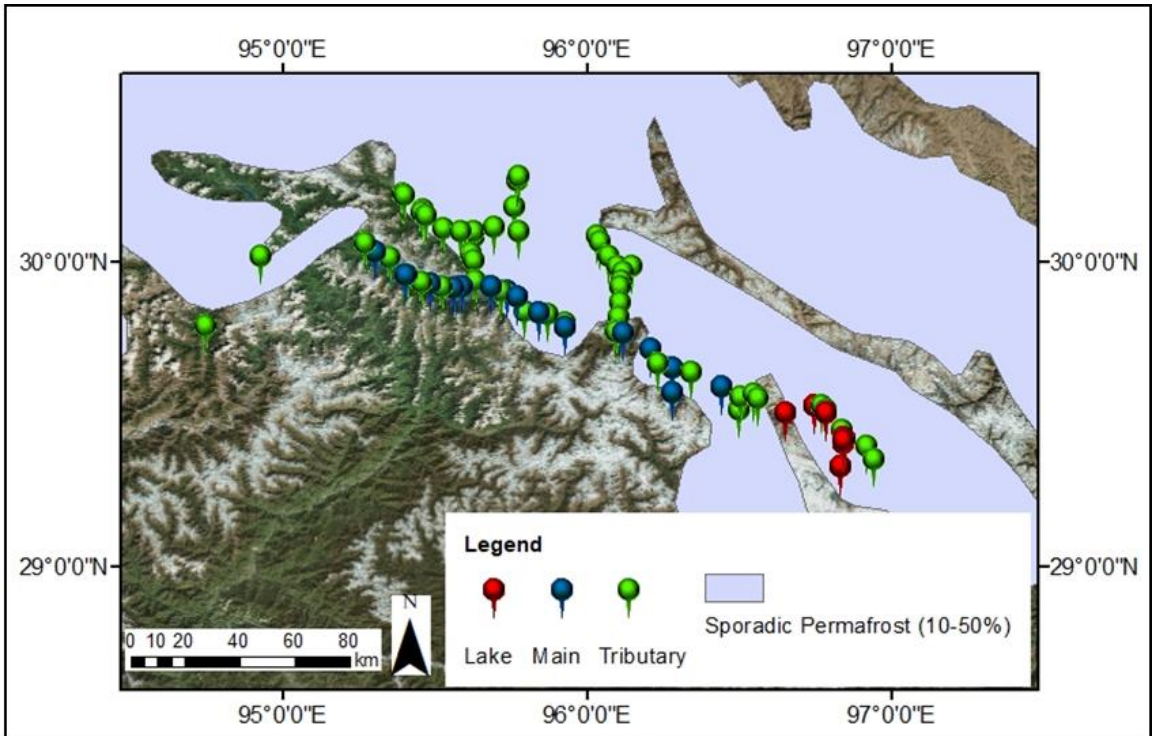

Figure 22: Map of sampling sites showing sporadic permafrost (10-50%). Map created with ArcGIS; permafrost data from NOAA (2016).

Optical techniques capture fluorescent DOM (FDOM) which makes up an unknown fraction of the total DOM pool (Stubbins et al., 2014). Molecular level techniques can be used to define the total DOM pool. Comparing PARAFAC model fluorescence components with FT-ICR-MS data for 22 freshwater samples, Stubbins et al. (2014) discover less than half of the total formulas from FT-ICR-MS analysis were represented by the identified fluorescence components. This gap between FT-ICR-MS and fluorescence data highlights that characterizing only FDOM may not encapsulate all the variation of the total DOM pool. Equally important, FT-ICR-MS analysis requires solid-phase extraction of DOM, and Wunsch et al. (2018) find that discrepancies exist between bulk water samples and DOM extracts and reveal that solid-phase extraction is qualitatively selective and results in homogenization of DOM extracts compared to original bulk water samples. The 5 component PARAFAC model created with the 179 Parlung Zangbo main stem, tributary, and lake samples produced a protein-dominated DOM pool. While a proteinaceous DOM pool has been described in glacial environments previously (Barker et al., 2009; Hood et al., 2009; Dubnick, et al., 2010), FT-ICR-MS data suggests a DOM pool dominated by lignin-like compounds for the Parlung Zangbo River. Milner et al. (2017) find organic matter locked in glacial ice to be extremely diverse with both proteinaceous and lignin-like DOM abundant. The inconsistency between the PARAFAC model and FT-ICR-MS results of whether proteinaceous or lignin-like DOM dominate the DOM pool may be caused by a combination of the lack of representation of non-fluorescing DOM in optical measurements and the bias of DOM extracts used for FT-ICR-MS analysis. There is some correlation between EEM parameters and FT-ICR-MS parameters. % F_{C1}, a humic-like component, is positively correlated with % lignin-like and DBE and negatively correlated with % protein-like (Table 6).

The average DOC concentration of our samples, 3.08 mg/L, is on the low end of the spectrum for rivers globally which typically ranges from 0.5 to 50 mg/L (Stubbins et al., 2014). Low DOC concentrations have been found in Tibetan rivers in previous studies (Qu et al., 2017). Increasing contributions of carbon from permafrost thaw and glacial melt in the future has the potential to raise DOC concentrations in these rivers. Hood et al. (2009) find glaciated watersheds are the source of some of the oldest and most labile DOM, and the extent of glacial coverage in the Parlung Zangbo watershed can be seen in Figure 21. Our incubation experiments were setup to show the impact of increasing temperatures on DOM utilization. Results show total DOM utilization for all samples is highest at 17°C and lowest at 25°C, and this trend is consistent when total DOM utilization for Main samples is compared at each temperature. DOM utilization was expected to increase with increasing temperature, which holds true if comparing the 11°C experiment with the 17°C experiment. However, DOM utilization decreases with increasing temperature when comparing 11°C to 25°C and 17°C to 25°C. These results suggest DOM utilization may increase with increasing temperature until reaching a tipping point, somewhere between 11°C and 25°C, where DOM utilization starts to decrease as temperature exceeds this tipping point. Nevertheless, comparison of the 17°C experiment with the 11°C and 25°C experiments must be carried out with the acknowledgement that, due to space limitations, the 17°C experiment was not performed simultaneously with the other two experiments, and thus, a separate bacterial inoculum, prepared in the same manner with the same soil, was used to inoculate the 17°C samples. In the 25°C experiment, Lake samples had greater DOM utilization, and for the same experiment, Fmax3, microbially derived DOM, had the greatest increase in Lake samples. Lake samples are characterized by higher β:α, more fresh DOM, and lower E2:E3, larger molecules; these indices may help predict greater DOM utilization. Coincident with the

influence of temperature on DOM utilization, increases in glacial melt and thawing permafrost will alter the characteristics and quantity of DOM present in the river system. For example, Qu et al. (2017) find periods of high discharge export ^{14}C-depleted/old carbon from permafrost regions of the Tibetan Plateau. Shifts in the characteristics and quantity of DOM present in the river system will also impact bacteria utilization, though these experiments only considered temperature.

CONCLUSIONS

With increasing emphasis on a changing climate, scientific studies are putting the global carbon cycle at center stage. The role of river networks as transporters, sinks, and transformers of carbon make these systems of primary interest. Since DOM comprises most of the organic carbon in river networks, characterizing the amount, source, and biodegradability of DOM present in a river network assists in describing the cycling of carbon. The age, quantity, and reactivity of the DOM pool in these river networks have the potential to shift considerably with climatic changes. Potential shifts in the DOM pool encourages present-day characterization to create a baseline for predictions of future conditions. Optical measurements suggest significant contributions of supraglacial meltwater to the Parlung Zangbo River creating a proteinaceous DOM pool; while FT-ICR-MS analysis suggests significant contributions of plant and soil matter to the river creating DOM pool dominated by lignin-like compounds. These results suggest a mixture of compounds of diverse origins and compositions in Tibet rivers. With expected increases in glacial meltwater in the future, greater quantities of microbial DOM and N-rich DOM are expected to be delivered to the river. PCA analysis suggests %CHON, β:α, DOC, AI_{mod}, and %CAS can serve as indicators of DOM released from glacial melting.

Increasing temperatures on the Tibetan Plateau is accelerating glacier melt and could trigger significant permafrost thawing. Both events will release more carbon and other nutrients to river networks on the plateau. Increased carbon concentrations coupled with higher temperatures is expected to catalyze bacteria utilization of DOM. Incubation experiments, manipulating temperature only, suggest bacteria utilization may increase until reaching an

optimum temperature, that if exceeded, bacteria utilization will start to decrease. In the 25°C experiment, Lake samples, the grouping with the highest β:α, most fresh DOM, had the greatest DOM utilization, supporting fresher DOM is more labile. Also, in the 25°C experiment, C1 had the smallest DOM utilization compared to all other components. C1 is composed of humic-like compounds, potentially OM degradation products, and is more recalcitrant compared to the other DOM components. Additional experiments are needed to explore how adding nutrients will impact bacteria utilization and if the trend of increasing up to an optimum temperature is continued.

Referred to as the "Water Tower of Asia," the Tibetan Plateau is the source of many of Asia's large rivers, namely the Yarlung Zangbo River, and supports hundreds of millions of people. The Tibetan Plateau is also the highest and most extensive plateau in the world, and consequently, is experiencing warming at a faster rate than the rest of world. As a result, the Tibetan Plateau can be studied as a barometer for climate change, assuming climatic shifts the Tibetan Plateau is experiencing today will eventually be experienced around the world. This study characterizing DOM of the Parlung Zangbo River lays the groundwork to understand the impacts of changing climate on carbon dynamics within alpine drainage networks.

REFERENCES

Addinsoft (2019). XLSTAT statistical and data analysis solution. Boston, USA. https://www.xlstat.com.

Barker, J.D., Sharp, M.J., and Turner, R.J., 2009, Using synchronous fluorescence spectroscopy and principal components analysis to monitor dissolved organic matter dynamics in a glacier system: Hydrological Processes, v. 23, p. 1487-1500, doi:10.1002/hyp.7274.

Brandão, L.P.M., Brighenti, L.S., Staehr, P.A., Asmala, E., Massicotte, P., Tonetta, D., Barbosa, F.A.R., Pujoni, D., and Bezerra-Neto, J.F., 2018, Distinctive effects of allochthonous and autochthonous organic matter on CDOM spectra in a tropical lake: Biogeosciences, v. 15, p. 2931-2943, doi: 10.5194/bg-15-2931-2018.

Choi, C.E., Cui, Y., Au, K.Y.K., Liu, H., Wang, J., Liu, D., and Wang, H., 2018, Case Study: Effects of a partial-debris dam on riverbank erosion in the Parlung Tsangpo River, China: Water, v. 10, no. 250, p. 1-12, doi: 10.3390/w10030250.

Coble P.G., 2007, Marine optical biogeochemistry: the chemistry of ocean color: Chemical Reviews, v. 107(2), p. 402-418.

Cory, R. M. and McKnight, D.M., 2005, Fluorescence spectroscopy reveals ubiquitous presence of oxidized and reduced quinones in dissolved organic matter: Environmental Science & Technology, v. 39, p. 8142-8149.

Creed, I.F., Bergstrom, A.K., Trick, C.G., Grimm, N.B., Hessen, D.O, Karlsson, J., Kidd, K.A., Kritzberg, E., McKnight, D.M., Freeman, E.C., Senar, O.E., Andersson, A., Ask, J., Berggren, M., Cherif, M., Giesler, R., Hotchkiss, E.R., Kortelainen, P., Palta, M.M., Vrede, T., and Weyhenmeyer, G.A., 2018, Global change-driven effects on dissolved organic matter composition: Implications for food webs of northern lakes: Global Change Biology, v. 24, p. 3692-3714, doi: 10.1111/gcb.14129.

De Haan H and De Boer T, 1987, Applicability of light absorbance and fluorescence as measures of concentration and molecular size of dissolved organic carbon in humic Lake Tjeukemeer: Water Resources, v. 21, p. 731-734.

Dittmar, T., Koch, B., Hertkorn, N., and Kattner, G., 2008, A simple and efficient method for solid-phase extraction of dissolved organic matter (SPE-DOM) from seawater: Limnology and Oceanography: Methods, v. 6, p. 230-235.

Dubnick, A., Barker, J., Sharp, M., Wadham, J., Lis, G., Telling, J., Fitzsimons, S., and Jackson,

M., 2010, Characterization of dissolved organic matter (DOM) from glacial environments using total fluorescence spectroscopy and parallel factor analysis: Annals of Glaciology, v. 51(56), p. 111-122.

Fellman, J. B., Spencer, R. G. M., Hernes, P. J., Edwards, R. T., D'Amore, D. V., and Hood, E., 2010, The impact of glacier runoff on the biodegradability and biochemical composition of terrigenous dissolved organic matter in near-shore marine ecosystems: Marine Chemistry, v. 121, p.112-122.

Fountain, A.G., Campbell, J.L., Schuur, E.A.G., Stammerjohn, S.E., Williams, M.W., and Ducklow, H.W., 2012, The disappearing cryosphere: impacts and ecosystem responses to rapid cryosphere loss: BioScience, v. 62, p. 405-415.

Hansell, D.A. and Carlson, C.A., 2002, Biogeochemistry of Marine Dissolved Organic Matter: Chapter 4: Academic Press, San Diego.

Hansen, A.M., Kraus, T.E.C., Pellerin, B.A., Fleck, J.A., Downing, B.D., and Bergamaschi, B.A., 2016, Optical properties of dissolved organic matter (DOM): Effects of biological and photolytic degradation: Limnology and Oceanography, v. 61, p. 1015-1032.

Hood, E. and Berner, L., 2009, Effects of changing glacial coverage on the physical and biogeochemical properties of coastal streams in southeastern Alaska: Journal of Geophysical Research, v. 114, p. 1-10.

Hood, E., Fellman, J., Spencer, R.G., Hernes, P.J., Edwards, R., D'Amore, D., and Scott, D., 2009, Glaciers as a source of ancient and labile organic matter to the marine environment: Nature, v. 462, no. 7276, p. 1044-1047.

Hockaday, W.C., Purcell, J.M., Marshall, A.G., Baldock, J.A., and Hatcher, P.G., 2009, Electrospray and photoionization mass spectrometry for the characterization of organic matter in natural waters: a qualitative assessment: Limnology and Oceanography: Methods, v. 7, p. 81-95.

Huang, X., Sillanpää, M., Gjessing, E.T., and Vogt, R.D., 2009a, Water quality in the Southern Tibetan Plateau: Chemical evaluation of the Yarlung Tsangpo (Brahmaputra): River Research and Applications, v. 27, p. 113-121, doi: 10.1002/rra.1332.

Huang, X., Sillanpää, M., Gjessing, E.T., and Vogt, R.D., 2009b, Water quality in the Tibetan Plateau: Major ions and trace elements in the headwaters of four major Asian rivers: Science of the Total Environment, v. 407, no. 24, p. 6242–6254, doi: 10.1016/j.scitotenv.2009.09.001.

Huguet, A., Vacher, L., Relexans, S., Saubusse, S., Froidefond, J.M., and Parlanti E., 2009, Properties of fluorescent dissolved organic matter in the Gironde Estuary: Organic Geochemistry, v. 40, p. 706-719, doi: 10.1016/j.orggeochem.2009.03.002.

Jaffé, R., McKnight, D., Maie, N., Cory, R., Mcdowell, W.H., and Campbell, J.L., 2008, Spatial

and temporal variations in DOM composition in ecosystems: The importance of long-term monitoring of optical properties: Journal of Geophysical Research: Biogeosciences, 113: G04032, doi: 10.1029/2008JG000683.

Li, F., Xu, Z., Liu, W., and Zhang, Y., 2014, The impact of climate change on runoff in the Yarlung Tsangpo River basin in the Tibetan Plateau: Stoch Environ Res Risk Assess, v. 28, p. 517-526, doi: 10.1007/s00477-013-0769-z.

Liu, Z., Yao, Z., Huang, H., Wu, S., and Liu, G., 2012, Land use and climate change and their impacts on runoff in the Yarlung Zangbo River Basin, China: Land Degradation and Development, v. 25, p. 203-215, doi: 10.1002/Idr.1159.

Lu, Y.H., Bauer, J.E., Canuel, E.A., Yamashita, Y., Chambers, R.M., and Jaffe, R., 2013, Photochemical and microbial alteration of dissolved organic matter in temperate headwater streams associated with different land use: Journal of Geophysical Research: Biogeosciences, v. 118, p. 566-580, doi: 10.1002/jgrg.20048.

Lu, Y. H., Edmonds, J.W., Yamashita, Y., Zhou, B., Jaegge, A., and Baxley, M., 2015a, Spatial variation in the origin and reactivity of dissolved organic matter in Oregon-Washington coastal waters: Ocean Dynamics, v. 65, p.17-32.

Lu, Y.H., Li, X., Mesfioui, R., Bauer, J.E., Chambers, R.M., Canuel, E.A., and Hatcher, P.G., 2015b, Use of ESI-FTICR-MS to characterize dissolved organic matter in headwater streams draining forest-dominated and pasture-dominated watersheds: PLoS ONE 10(12): e0145639. https://doi.org/10.1371/journal.pone.0145639.

McKnight, D.M., Boyer, E.W., Westerhoff, P.K., Doran, P.T., Kulbe, T., and Andersen, D.T., 2001, Spectrofluorometric characterization of dissolved organic matter for indication of precursor organic material and aromaticity: Limnology and Oceanography, v. 46, p. 38-48, doi: 104319/lo.2001.46.1.0038.

Milner, A.M., Khamis, K., Battin, T.J., Brittain, J.E., Barrand, N.E., Fureder, L., Cauvy-Fraunie, S., Gislason, G.M., Jacobsen, D., Hannah, D.M., Hodson, A.J., Hood, E., Lencioni, V., Olafsson, J.S., Robinson, C.T., Tranter, M., and Brown, L.E., 2017, Glacier shrinkage driving global changes in downstream systems: Proceedings of the National Academy of Sciences, p. 1-9.

Mopper and Schultz, 1993, Fluorescence as a possible tool for studying the nature and water column distribution of DOC components: Marine Chemistry, v. 41, p. 229-238.

Murphy, K.R., Stedmon, C.A., Graeber F., and Bro, R., 2013, Fluorescence spectroscopy and multi-way techniques: PARAFAC Analytic Methods, v. 5, p. 6557-6566.

Ohno, T., He, Z., Honeycutt, C.W., Sleighter, R.L., Hatcher, P.G., 2010, Ultrahigh resolution mass spectrometry and indicator species analysis to identify marker components of soil- and plant biomass-derived organic matter fractions: Env. Science and Tech., v. 44, p. 8594-8600.

Parlanti, E., Worz, K., Geoffroy, L., and Lamotte, M., 2000, Dissolved organic matter fluorescence spectroscopy as a tool to estimate biological activity in a coastal zone submitted to anthropogenic inputs: Organic Geochemistry, v. 31, p. 1765-1781, doi:10.1016/S0146-6380(00)00124-8.

Qu, B., Sillanpää, M., Li, C., Kang, S., Stubbins, A., Yan, F., Aho, K.S., Zhou, F., and Raymond, P., 2017, Aged dissolved organic carbon exported from rivers of the Tibetan Plateau: PLoS ONE 12(5): e0178166. https://doi.org/10.1371/journal.pone.0178166.

Raymond, P.A., Saiers, J.E., and Sobczak, W.V., 2016, Hydrological and biochemical controls on watershed dissolved organic matter transport: pulse-shunt concept: Ecology, v. 97, p. 5-16.

Sankar, M.S., Dash, P., Singh, S., Lu, Y.H., Mercer, A.E., and Chen, S., 2018, Effect of phot-biodegradation on the biochemical cycling of dissolved organic matter across diverse surface water bodies: Journal of Environmental Sciences, doi:10.1016/j.jes.2018.06.021.

Shang, P., Lu, Y., Du, Y., Jaffe, R., Findlay, R., and Wynn, A., 2018, Climatic and watershed controls of dissolved organic matter variation in streams across a gradient of agricultural land use: Science of the Total Environment, v. 612, p.1442-1453, doi: 10.1016/j.scitotenv.2017.08.322.

Shi, Y., Gao, X., Zhang, D., Giorgi, F., 2011, Climate change over the Yarlung Zangbo-Brahmaputra River Basin in the 21st century as simulated by a high resolution regional climate model: Quaternary International, v. 244, p. 159-168, doi: 20.1016/j.quaint.2011.01.041.

Singh, S., Inamdar, S., and Scott, D., 2013, Comparision of two PARAFAC models of dissolved organic matter fluorescence for a mid-atlantic forested watershed in the USA: Journal of Ecosystems, v. 2013, doi:10.1155/2013/532424.

Spencer, R.G., Bolton, L., and Baker, A., 2007, Freeze/thaw and pH effects on freshwater dissolved organic matter fluorescence and absorbance properties from a number of UK locations: Water Resources, v. 41, p. 2941-2950.

Stedmon, C.A., Markager, S., Søndergaard, M., Vang, T., Laubel, A., Borch, N.H., and Windelin, A., 2006, Dissolved organic matter (DOM) export to a temperate estuary: seasonal variations and implications of land use: Estuaries and Coasts, v. 29, p. 388-400.

Stubbins, A., Lapierre, J.F., Berggren, M., Prairie, Y.T., Dittmar, T., and Giorgio, P.A., 2014, What's in an EEM? Molecular signatures associated with dissolved organic fluorescence in boreal Canada: Environmental Science and Technology, v. 48, p. 10598-10606, doi: 10.1021/es502086e.

Wilson, H.F., and Xenopoulos, M.A., 2009, Effects of agricultural land use on the composition of fluvial dissolved organic matter: Nature Geoscience, v. 2, p. 37-41.

Wünsch, U.J., Murphy, K.R., and Stedmon, C.A., 2017, The one-sample PARAFAC approach reveals molecular size distributions of fluorescent components in dissolved organic matter: Environmental Science Technology, v. 51(20), p. 1190-11908.

Yao, T.D., Li, Z.G., Yang, W., Guo, X.J., Zhu, L.P., Kang, S.C., Wu, Y.H., and Yu, W.S., 2010, Glacial distribution and mass balance in the Yarlung Zangbo River and its influence on lakes: Chinese Science Bulletin, v. 55, no. 20, p. 2072-2078, doi: 10.1007/s11434-010-3213-5.

Yang, K., Wu, H., Qin, J., Lin, C., Tang, W., and Chen, Y., 2014, Recent climate changes over the Tibetan Plateau and their impacts on energy and water cycle: a review: Global and Planetary Change, v. 112, p. 79-91.

Zhou, S.Z., Xu, L.B., Colgan, P.M., Mickelson, D.M., Wang, X.L., Wang, J., and Zhong, W., 2007, Cosmogenic ^{10}Be dating of Guxiang and Baiyu Glaciations: Chinese Science Bulletin, v. 52, no. 10, p. 1387-1393, doi: 10.1007/s11434-007-0208-y.